Computational Materials Science 210 (2022) 111474

Contents lists available at ScienceDirect

Computational Materials Science

journal homepage: www.elsevier.com/locate/commatsci

Full Length Article

The role of entropy and enthalpy in high entropy carbides

Xiaochuan Tang [a,*], Gregory B. Thompson [b], Kaka Ma [a,c], Christopher R. Weinberger [a,c]

[a] Department of Mechanical Engineering, Colorado State University, Fort Collins, CO 80523, USA
[b] Department of Metallurgical and Materials Engineering, University of Alabama, Tuscaloosa, AL 35487, USA
[c] School of Advanced Materials Discovery, Colorado State University, Fort Collins, CO 80523, USA

ARTICLE INFO

Keywords:
DFT
Transition metal carbides
Thermodynamic stability

ABSTRACT

The thermodynamic stability of equiatomic mixed carbides, commonly referred to as high entropy carbides (HECs), is investigated via the CALculation of PHAse Diagrams (CALPHAD) approach for mixed carbides consisting of the group IVB and VB transition metal carbides as well as tungsten carbide. The Gibbs free energy of the B1-structured mixed carbides is computed using the compound energy formalism while that of the B_h-structured mixed carbides is evaluated using a point-defect model. The required thermodynamic data for the CALPHAD approach are obtained from density functional theory calculations and the Debye-Grüneisen model. The lower temperature limit at which the HECs mix in thermodynamic equilibrium is determined via numerical and analytical approaches. We find that enthalpy of mixing is at least as important as configurational mixing entropy in these mixed transition metal carbide compounds. The lower limit temperature where an equiatomic solid solution is present is largely independent of the number of components with the only exception being solutions containing tungsten carbide, where a weak temperature dependence is noted. Furthermore, the only equiatomic solid solutions that are thermodynamically stable below approximately 1000 K are those stabilized by enthalpy alone, indicating that many currently fabricated HECs are not at equilibrium at room temperature. Collectively, our results demonstrate that the formation of these carbides is controlled by the competition between entropy and enthalpy, or enthalpy alone, and thus these materials should be referred to as multi-principal component carbides since the former terminology can be misleading.

1. Introduction

The transition metal carbides (TMCs), a family of ultra-high-temperature ceramics (UHTCs), exhibit not only high melting temperature but also high hardness and moderate oxidization resistance because of their nature of mixed covalent-metallic or covalent-metallic-ionic bonds [1–3]. To further enhance the material properties, the concept of mixing multiple metal species onto a single phase lattice has been proposed [4–6], and termed high entropy carbides (HECs), which makes these compounds fall into the category of 'high entropy ceramics' [7]. These so-called high entropy ceramics are analogous to high entropy alloys (HEA) [8,9] which usually consist of four or five principal components. The transition metal carbides are typically interstitial compounds where the metal atoms (M) form a cubic or hexagonal sublattice with the carbon (C) atoms occupying the interstitials. In the case of the group IVB and VB carbides, there exists wide stoichiometries of the rock-salt (B1) structure, MC_{1-x}, where x can range from 0.5 to 1 [3,10]. This potential range of carbon content and the number of transition metals creates a large design space for the design of HECs [11].

The experimental studies of HECs started with the mixture of 4 or 5 B1-structured unary carbides, such as $(Ti_{1/4}Zr_{1/4}Hf_{1/4}Ta_{1/4})C$ [12], $(Zr_{1/4}Hf_{1/4}Nb_{1/4}Ta_{1/4})C$ [12–14], $(Ti_{1/5}Zr_{1/5}Hf_{1/5}Nb_{1/5}Ta_{1/5})C$ [15–17] and $(Ti_{1/5}Hf_{1/5}V_{1/5}Nb_{1/5}Ta_{1/5})C$ [6,17] via consolidation of mechanically alloyed (ball-milled) equimolar unary carbide powders. Compared to unary carbides, these HECs exhibited higher hardness (by 10%~20%) [12], increased yield and failure strength [14], and enhanced oxidation resistance [16]. Further enhancement of the mechanical properties of HECs, i.e. ductility and hardness, was found in the fabricated B1-structured multicomponent carbides by stabilizing the typically B_h-structured unary carbides MoC and WC [17–19]. However, unlike these reports of the synthesis of HECs, the heat treatment of mixed non-equimolar unary carbide powders suggest the existence of large miscibility gaps even at elevated temperatures (~1500 °C) in multicomponent carbide systems, such as Nb-Ti-V-C [20] and Co-Ti-V-W-Zr-C [21]. These reports suggest that the thermodynamic stability of single-phase

* Corresponding author.
E-mail addresses: xtang@ucdavis.edu (X. Tang), gthompson@eng.ua.edu (G.B. Thompson).

https://doi.org/10.1016/j.commatsci.2022.111474
Received 15 March 2022; Received in revised form 22 April 2022; Accepted 23 April 2022
0927-0256/© 2022 Elsevier B.V. All rights reserved.

HECs is questionable at room temperature. In addition, there is still a lack of solid evidence, *e.g.* quantitative evaluation of the mixing entropy, to support the previous hypothesis that the mixing entropy in the solid solution results in the stability of these so-called HECs. Other factors that may give rise to the thermodynamic stability of HECs include the mixing enthalpy, the structure and elasticity of the carbide components, etc. and should also be considered for further investigation. Therefore, the terminology high entropy carbide (or high entropy ceramic) may not be an accurate description of these materials, though we will utilize this name throughout this manuscript since this is the only name used to-date.

Two general methods have been adopted in the computational studies of HECs: the descriptor method [15,22,23] and the calculation of phase diagrams (CALPHAD) [24,25]. The descriptor method uses a material-specific property to describe the solubility of the multicomponent carbides, which is akin to the Hume-Rothery rules used for alloys. Using this idea, Yang *et al.* used the degree of lattice-distortion as the descriptor to predict the phase stability of the high entropy carbides $(Hf_{1/5}Nb_{1/5}Ta_{1/5}Ti_{1/5}Zr_{1/5})C$ by means of density functional theory (DFT) [15]. Ye *et al.* concluded the stability of $(Nb_{1/4}Ti_{1/4}V_{1/4}Zr_{1/4})C$ based on the small mixing enthalpy obtained from *ab-initio* calculations [22]. The descriptor of entropy forming ability (EFA) was used by Sarker *et al.* to relate the standard deviation in the enthalpy of an equiatomic mixed carbide with different atomic configurations [23]. They assumed that a smaller standard deviation in the enthalpy indicated a larger configurational entropy, which was suggested to improve the phase stability of the mixed carbides by lowering the total Gibbs free energy. These authors used this descriptor to investigate the phase stability of HECs with combinations of 8 metal elements (Ti, Zr, Hf, V, Nb, Ta, Cr, Mo, W) and found that the consistent results were obtained by using both EFA and degree of lattice-distortion as descriptors. The descriptor method's advantages are its simple implementation and the fast prediction of phase stability. But the choice of the descriptor is empirical and lacks an explicit relationship with the Gibbs free energy.

Unlike the descriptor method, the CALPHAD approach computes the Gibbs free energy directly and constructs the phase diagrams of the mixed carbides with all compositions at different temperatures. The use of the CALPHAD approach requires thermodynamic data, which can be either assessed from experiments [20,21,24] or evaluated via computation [25]. Servant *et al.* used experimentally assessed thermodynamic data and computed the phase diagrams of the B1-structured binary carbides (M_i-M_j-C), consisting of some of the group IVB and VB carbides and CrC [24] but did not extend their results to HECs. Markström *et al.* also investigated some of the B1-structured binary carbides using the CALPHAD approach but instead used thermodynamic data from *ab-initio* calculations rather than experiments [25]. A similar approach was taken by Ivaschenko *et al.* [26] who included finite temperature effects via phonons. However, none of these studies have examined the thermodynamics of all the transition metal carbides for pseudo-ternary systems and above, which is necessary to understand the role entropy plays in forming HECs.

While experimental studies have demonstrated the ability to synthesize HECs and theoretical studies have provided insight into the stability of these compounds, the thermodynamic stability of HECs has not been definitively addressed or answered. Specifically, no one has, to-date, computed the temperatures required to synthesize equiatomic HECs with more than three elements and thus the true thermodynamic stability of these materials remains in question. To address this knowledge gap, in this work we use the CALPHAD approach to compute the thermodynamic stability of equiatomic mixed HECs directly using the Gibbs free energy for all the group IVB, VB and W transition metals. For consistency, the required thermodynamic data in our CALPHAD approach was first obtained at 0 K from *ab-initio* calculations using DFT [27] and then evaluated at finite temperatures using the Debye-Grüneisen model [28–30]. The Gibbs free energy of the B1-structured mixed carbides was computed using the classical compound energy formalism while that of the B_h-structured mixed carbides was evaluated using the point-defect model. This allows for the determination of the lower limit temperature at which the HECs will mix in thermodynamic equilibrium via numerical and analytical approaches. This approach will also allow for a connection between specific carbide systems used to form the solution and the resulting thermodynamic properties. The collective results in this study not only evaluate the thermodynamic stability of HECs; they also provide direct insight into the competition between entropy and enthalpy and guidance for material selection in HECs.

2. Methodology

2.1. Model development

2.1.1. Basic formalisms in phase equilibrium

In this study, we examined a solution of stoichiometric mixed carbides, equal fraction metal and carbon atoms, with N metal components denoted as $(M_{1x_1}M_{2x_2}\cdots M_{Nx_N})C$, where the metal element M_i has a corresponding molar fraction x_i. The thermodynamic stability of this compound is determined by its molar Gibbs free energy, which is related to x_i via the chemical potential μ_i [31]:

$$G = \sum_{i=1}^{N} x_i\mu_i, \sum_{i=1}^{N} x_i = 1. \tag{1}$$

Using the constraint of the molar fractions, the molar Gibbs free energy can be written as a function of $N-1$ variables by substituting $x_1 = 1 - \sum_{i=2}^{N} x_i$ so that the chemical potential of each component can be computed as:

$$\mu_1 = G - \sum_{j=2}^{N} \left(\frac{\partial G}{\partial x_j}\right)_{x_k(k\neq j)}, \tag{2}$$

$$\mu_i = G - \sum_{j=2}^{N} x_j \left(\frac{\partial G}{\partial x_j}\right)_{x_k(k\neq j)} + \left(\frac{\partial G}{\partial x_i}\right)_{x_k(k\neq i)}. \tag{3}$$

In general, a system consisting of multiple components may undergo phase separation, which could lower the overall Gibbs free energy by splitting the system into weighted phases. Assuming a two-phase equilibrium exists in a multi-component system, the composition of each phase is determined by the equality of chemical potentials:

$$\mu_i^{\alpha}\left(x_1^{\alpha}, x_2^{\alpha}, \cdots x_N^{\alpha}\right) = \mu_i^{\beta}\left(x_1^{\beta}, x_2^{\beta}, \cdots x_N^{\beta}\right), \tag{4}$$

where α and β denote the two different phases.

While the above discussion is generally true for computational thermodynamics, we have two specific cases that arise in the transition metal carbides we study here. In the case of mixing only group IVB and VB carbides, all components share the same rock-salt structure (the B1 structure). Thus, it is possible to either form a single B1 phase, or to phase separate into two or more phases, all of them with the B1 structure. In this case, the molar Gibbs free energy $G(x_2, x_3, \cdots x_N)$ is a continuous function over all the compositions but has the potential to exhibit regions of concavity, which is associated with spinodal decomposition [32]. The spinodal-decomposition region, i.e. the spinodes, can be determined from the Hessian matrix M of the Gibbs free energy, *e.g.*:

$$M_{ij}(x_2, x_3, \cdots x_N) = \frac{\partial^2 G}{\partial x_i \partial x_j}, (i,j = 2, \cdots N). \tag{5}$$

Consequently, the spinodes are determined by $\det(M) = 0$. Thus, there are two important temperatures to consider when discussing the equiatomic mixing of the B1 carbides: the minimum temperature at which they mix in thermodynamic equilibrium, T_{eqv}, and the temperature at which there is no spinodal decomposition, T_{eqv}^{sd}. T_{eqv} can be most easily understood and computed for a large number of carbides as the highest temperature at which Eq. (4) has a solution for two different B1

phases. Similarly, T^{sd}_{eqv} can be found simply be determining the largest temperature at which Eq. (5) has a zero determinant at the multicomponent equiatomic composition.

The second case involves mixing the B1-structured carbides with WC. In this case, we have to consider equilibrium between two phases with different structures, the B1 structure and B_h structure, and thus two discontinuous Gibbs free energy curves. The temperature, T_{eqv}, is therefore either controlled by the phase equilibrium between the B1 and B_h phases or it may still be controlled by the phase separation between two B1 phases. In this case, Eq. (4) must be directly used for the equilibrium of the B1 and B_h structures and the composition steps used to check Eq. (4) are 0.01.

2.1.2. Thermodynamic models for the mixture of the B1-structured carbides

The Gibbs free energy of the mixed B1-structured carbides $\left(M_{1x_1^\alpha}M_{2x_2^\alpha}\cdots M_{Nx_N^\alpha}\right)C$ can be written using the compound energy formalism [33] as:

$$G^\alpha(T)=\sum_{i=1}^{N}x_i^\alpha G^\alpha_{M_iC}(T)+G^\alpha_{mix}(T)+Tk_B\sum_{i=1}^{N}x_i^\alpha \ln x_i^\alpha, \tag{6}$$

where α denotes the B1 phase, T is the temperature, k_B is Boltzmann's constant, $G^\alpha_{M_iC}$ represents the Gibbs free energy for the unary B1-structured carbide M_iC, and G^α_{mix} represents the excess mixing Gibbs free energy of G^α. In Eq. (6), the Gibbs free energy is the energy per formula unit (f.u.) of the carbide and the third term $k_B\sum_{i=1}^{N}x_i^\alpha \ln x_i^\alpha$ is the mixing of configurational entropy. We note that the unit of the Gibbs free energy can be converted into energy per mole by multiplying the Avogadro's number in Eq. (6) and both units are used in the plots in the following results. Similarly, the total enthalpy of the mixed carbide at 0 K is:

$$H^{\alpha^*}=\sum_{i=1}^{N}x_i^\alpha H^{\alpha^*}_{M_iC}+H^{\alpha^*}_{mix}, \tag{7}$$

where an asterisk in this paper denotes a thermodynamic property evaluated at 0 K. The term G^α_{mix} in Eq. (6) and $H^{\alpha^*}_{mix}$ in Eq. (7) represent the solubility amongst the unary carbides, which can be approximated as:

$$H^{\alpha^*}_{mix}=\frac{1}{2}\sum_{i=1}^{N}\sum_{j\neq i}^{N}x_i^\alpha x_j^\alpha L^{\alpha^*}_{M_iC-M_jC}, \tag{8}$$

$$G^\alpha_{mix}(T)=\frac{1}{2}\sum_{i=1}^{N}\sum_{j\neq i}^{N}x_i^\alpha x_j^\alpha L^{\alpha}_{M_iC-M_jC}(T). \tag{9}$$

The $L^{\alpha^*}_{M_iC-M_jC}$ and $L^{\alpha}_{M_iC-M_jC}(T)$ terms in Eqs. (8) and (9) are the parameters representing the solubility of the binary carbides M_iC-M_jC, which are expressed using Redlich-Kister (RK) polynomials in this study:

$$L^{\alpha^*}_{M_iC-M_jC}=\sum_{k=0}^{K}L^{ak^*}_{M_iC-M_jC}\left(x_i^\alpha-x_j^\alpha\right)^k. \tag{10a}$$

$$L^{\alpha}_{M_iC-M_jC}(T)=\sum_{k=1}^{K}L^{ak}_{M_iC-M_jC}(T)\left(x_i^\alpha-x_j^\alpha\right)^k. \tag{10b}$$

The RK polynomials with $K=0$ and 1 are called regular and subregular solutions, respectively [33]. In this work, the values of $L^{ak^*}_{M_iC-M_jC}$ and $L^{ak}_{M_iC-M_jC}(T)$ in Eq. (10) are evaluated from *ab-initio* calculations as discussed in Sec. 2.2.

2.1.3. Thermodynamic models for the mixture of the B1-structured carbides and WC

Tungsten carbide (WC) can form two structures under different conditions. At room temperature, WC has the B_h structure where the metal atoms form a simple hexagonal sublattice and the carbon atoms fill the octahedral interstitials. At elevated temperatures, WC_{1-x} can form the rock-salt structure (the B1 structure), which can either form a single phase or coexist with the hexagonal-based W_2C and B_h WC. Between 2789 K and 3028 K, the composition range of the B1-structured WC_{1-x} is $0\le x\le 0.41$. Therefore, the solubility of B1 WC in other B1-structured carbides can be modelled by using the RK polynomials as shown in Eqs. (8)-(10). However, the solubility of W in the B1 structure at low temperatures is likely to be modest. In contrast, the group IVB and VB stoichiometric carbides do not form the B_h structure at any known temperatures, which means the solubility of the group IVB and VB carbides in B_h WC is likely very low. Therefore, we choose to model the B_h-structured mixed carbide as having a B_h WC matrix with substitutional metal atoms modeled as point defects. Using this model, the Gibbs free energy of the mixed carbide $\left(M_{1x_1^\beta}M_{2x_2^\beta}\cdots M_{Nx_N^\beta}W_{1-\sum_{i=1}^{N}x_i^\beta}\right)C$ is:

$$G^\beta(T)=\sum_{i=1}^{N}x_i^\beta\left[G^\alpha_{M_iC}(T)+\Delta G^\beta_{M_iC}(T)\right]+\left(1-\sum_{i=1}^{N}x_i^\beta\right)G^\beta_{WC}(T)+TS_{mix}, \tag{11}$$

$$S_{mix}=k_B\left[\sum_{i=1}^{N}x_i^\beta\ln x_i^\beta+\left(1-\sum_{i=1}^{N}x_i^\beta\right)\ln\left(1-\sum_{i=1}^{N}x_i^\beta\right)\right], \tag{12}$$

where β denotes the B_h phase and the term $\Delta G^\beta_{M_iC}(T)$ represents the excess energy of a single point defect (substitutional M_i atom). Similarly, the enthalpy at 0 K is:

$$H^{\beta^*}=\sum_{i=1}^{N}x_i^\beta\left[H^{\alpha^*}_{M_iC}+\Delta H^{\beta^*}_{M_iC}\right]+\left(1-\sum_{i=1}^{N}x_i^\beta\right)H^{\beta^*}_{WC}. \tag{13}$$

We expect that the concentration of group IVB and VB transition metals in the B_h phase will be low, and we choose to ignore the short-range interactions between the metal atoms. Thus, it is appropriate to model the enthalpy of mixing using a simple point defect model that neglects these interactions.

2.2. DFT calculations

In the aforementioned thermodynamic models, the enthalpy of the mixed carbides at low temperatures is calculated based on the parameters of the binary (two-component) carbides, including the parameters $L^{\alpha^*}_{M_iC-M_jC}$ in Eq. (8) and $\Delta H^{\beta^*}_{M_iC}$ in Eq. (13). To evaluate $L^{\alpha^*}_{M_iC-M_jC}$, DFT calculations were carried out on the B1-structured unary carbides (M_iC) and pseudo-binary carbides ($M_{i1\text{-}x}M_{jx}$)C. The use of supercells to compute properties using DFT always results in ordered structures due to the periodic boundary conditions inherent to the simulations. However, the mixed carbides presumably have disordered structures where the metal atoms are randomly distributed. Thus, to best represent random mixing we utilize the well-known special quasi-random structures (SQSs) in all of our DFT simulations. For the B1-structured pseudo-binary carbides, the published SQSs [34–36] for fcc lattice (metal sublattice) were used as supercells where $x=1/8, 1/4, 3/8, 1/2$ and the structures of ($M_{i1\text{-}x}M_{jx}$)C with $x>1/2$ are modelled by swapping the M_i and M_j atoms. Moreover, we also performed DFT calculations on the published SQSs for the ternary, quaternary, and quinary carbides with the following compositions: $(M_{i1/4}M_{j1/4}M_{k1/2})C$, $(M_{i1/3}M_{j1/3}M_{k1/3})C$, $(M_{i1/4}M_{j1/4}M_{k1/4}M_{l1/4})C$, and $(M_{i1/5}M_{j1/5}M_{k1/5}M_{l1/5}M_{m1/5})C$ [34] to provide validation of our use of only binary mixing parameters discussed below.

The DFT calculations were performed using the projected-augmented-wave (PAW) pseudopotentials [37,38] implemented in the Vienna ab-initio simulation package (VASP) [39–41]. The electron correlation energy was calculated using generalized gradient

approximation (GGA) with the Perdew-Burke-Ernzerhof (PBE) parameterizations [42,43]. The first order Methfessel-Paxton smearing scheme with the smearing of 0.2 eV was implemented on the electronic occupancy in the Brillouin zone. The energy cut-off of the plane-wave basis was set to be 600 eV and the density of the Monkhorst-Pack k-point mesh was chosen as $12 \times 12 \times 12$ for the B1-structured conventional unit cell and $18 \times 18 \times 20$ for the B_h-structured primitive unit cell. The electronic convergence criterion was chosen as 10^{-8} eV in order to obtain the accurate mixing enthalpy and structural relaxations were set to a tolerance of 10^{-7} eV.

To investigate solid solutions of the B_h-structured carbides, we at first generated SQSs of the B_h-structured $(M_{i1-x}W_x)C$ using the ATAT code [44,45] similar to what we did for the B1-structured binary carbides. After performing the DFT simulations, we found that the SQSs were mechanically unstable for $x \leq 7/8$, which was established by examining two features of the structures. First, we noted that the hexagonal metal sublattice deformed substantially into a rhombohedral sublattice after the full relaxation. Second, the dynamical matrices of the original structures were not positive definite. These results further supported our initial assumption that the solubility of the group IVB and VB metal elements (M_i) inside B_h WC is relatively low. In order to mitigate this issue, we instead developed the defect thermodynamic model discussed in section 2.1.3 and proceeded to evaluate the defect formation energies of group IVB and VB metal atoms in B_h WC. We created supercells that are a repetition of the B_h WC primitive cell where a single W atom was replaced by the metal atom M_i. Note that due to the periodicity of the cell, there solution has no dependence on which W atom is replaced. Then, those structures with a single point defect were fully relaxed and the ground-state energy was calculated in VASP using the aforementioned parameters. Finally, the excess energy $\Delta H^{\beta^*}_{M_iC}$ of a single point defect (metal atom) was determined using a standard convergence test with respect to the supercell size.

2.3. Debye-Grüneisen model

In the previous section, the thermodynamic parameters in our model were evaluated using DFT calculations at 0 K. To obtain the finite temperature parameters, here we choose to use the Debye-Grüneisen (DG) model to calculate the internal energy (E_D) and entropy (S_D) of phonons [28–30] as well as those of electrons (E_{el} and S_{el}). While the vibrational free energy can be computed from density functional theory by computing the Hessian matrix, this approach would prove to be extremely computationally expensive in this application since the Hessian would have to be computed for every composition studied. However, Lu *et al.* [30] have demonstrated that the Debye-Grüneisen model is indeed quite accurate in predicting the Gibbs free energies of the transition metal carbides and nitrides making this approach both accurate and computational tractable. Thus, we take this approach to compute the Gibbs free energies for our computational model.

To illustrate our approach, we will take a unary carbide M_iC as an example. First, a supercell of the unary carbide M_iC was fully relaxed using DFT simulations allowing the structure to relax under zero pressure to determine the equilibrium volume, V_0, per formula unit. Next, several DFT simulations of the M_iC supercells were carried out at different volumes that ranged between 0.85 V_0 to 1.15 V_0 so that the ground-state energy-volume relationship at zero Kelvin is established. This data was then fit to a Morse potential: $E_{DFT}(V)$. Then, the pressure (P) and the Debye temperature (θ_D) were computed as functions of volume using the Debye-Grüneisen model:

$$P(V) = -\frac{\partial E_{DFT}(V)}{\partial V}, \tag{14}$$

$$\theta_D(V) = \kappa(\nu)\frac{\hbar}{k_B\sqrt{2m}}\left(12\pi^2 N_A\right)^{\frac{1}{3}}V^{\frac{1}{2}}\left[-\frac{\partial P(V)}{\partial V} - \frac{2(\lambda+1)}{3}\frac{P(V)}{V}\right], \tag{15}$$

where $\hbar$ is the reduced Planck's constant, k_B is Boltzmann constant, N_A is Avogadro's number, and $m = (m_{Mi}m_C)^{1/2}$ is the equivalent mass; which is the geometric mean of the metal and carbon atomic masses. The parameter λ in Eq. (15) determines the model used to evaluate the Grüneisen parameter and corresponds to the approximation method of the model. The values λ can take are -1, 0, or 1, which correspond to the Slater approximation [46], Dugdale-MacDondald (DM) approximation [47], and the free-volume approximation [48], respectively. The coefficient $\kappa(\nu)$ of θ_D in Eq. (15) can be written as an empirical function of the Poisson ratio ν as:

$$\kappa(\nu) = \left\{\frac{2}{3}\left[\frac{2(1+\nu)}{3(1-2\nu)}\right]^{3/2} + \frac{1}{3}\left[\frac{1+\nu}{3(1-\nu)}\right]^{3/2}\right\}^{-1/3}. \tag{16}$$

Using the Debye temperature, the molar internal energy and molar entropy of phonons were computed as:

$$E_D(T,V) = \frac{9}{4}N_A k_B\theta_D + 6N_A k_B T D\left(\frac{\theta_D}{T}\right), \tag{17}$$

$$S_D(T,V) = 8N_A k_B D\left(\frac{\theta_D}{T}\right) - 6N_A k_B \ln\left(1 - e^{-\theta_D/T}\right), \tag{18}$$

where $D(\theta_D/T)$ in Eqs. (17) and (18) is the Debye function:

$$D\left(\frac{\theta_D}{T}\right) = 3\left(\frac{\theta_D}{T}\right)^{-3}\int_0^{\theta_D/T}\frac{x^3}{e^x - 1}\mathrm{d}x, \tag{19}$$

which goes to 1 at high temperatures, $T \gg \theta_D$, and becomes proportional to T^3 at low temperatures $T \ll \theta_D$. The equation of state $V(T)$ was determined via the minimization of the Helmholtz free energy $F(T,V)$ calculated from Eq. (20):

$$F(T,V) = E_{DFT}(V) + E_D(T,V) - TS_D(T,V) + E_{el}(T,V) - TS_{el}(T,V), \tag{20}$$

where $E_{el}(T,V)$ and $S_{el}(T,V)$ are the molar internal energy and molar entropy of the thermally excited electrons near the Fermi level. Since the electronic DOS is nearly independent of volume, $E_{el}(T,V)$ and $S_{el}(T,V)$ were computed at the equilibrium volume (V_0) from the fully relaxed supercell. Based on the equation of state, the Gibbs free energy at finite temperature is calculated as:

$$\begin{aligned} G[T,V(T)] = {} & E_{DFT}[V(T)] + E_D[T,V(T)] - TS_D[T,V(T)] + E_{el}(T,V_0) \\ & - TS_{el}(T,V_0) + \int_{V(0)}^{V(T)} P[V(T)]\mathrm{d}V(T) \end{aligned} \tag{21}$$

In this work, we computed $G(T)$ for all unary and binary carbides with the structures mentioned in Sec. 2.2. The electronic contribution (E_{el} and S_{el}) to the Helmholtz free energy $F(T,V)$ was computed using the density of electronic states (DOS) from DFT simulations. To be consistent, the Poisson ratio ν was also computed from DFT simulations by implementing the Voigt-Reuss-Hill approximation on the stiffness tensor [49]. We determined that the parameter λ in Eq. (15) should be taken to be 1 in this work by comparing our DFT results with experimental data of the thermal expansion coefficients and heat capacities [50–61]. The calculation of $F(T,V)$, including all the details and the comprehensive comparisons with the experimental data are shown in the *Supplemental Materials*. Using these as-computed Gibbs free energies at finite temperature, the thermodynamic parameters $L^{\alpha}_{M_iC-M_jC}(T)$ and $\Delta G^{\beta}_{M_iC}(T)$ in Eqs. (9)-(11) were obtained from standard fitting of the RK polynomials. Finally, with the temperature dependent RK parameters determined, the phase stability of the mixed carbides was investigated using the methodologies outlined in Sec. 2.1. Specifically, the calculation of thermodynamic properties was coded in PYTHON and PYCALPHAD [62] was used to compute phase equilibrium.

3. Results and discussion

3.1. Mixing among the B1-structured carbides

3.1.1. Ab-initio assessment at 0 K

The first step in our thermodynamic assessment of the equiatomic transition metal carbides is to determine the RK polynomials for the enthalpy of mixing at 0 K using DFT. As noted previously, we used SQSs to evaluate the enthalpy of formation of the mixed carbides. However, the question always arises regarding the effect of simulation cell distortions and atomic relaxations since the supercells are always periodic and won't exactly retain the cubic symmetry when complete structural relaxations are used in DFT. To examine this effect, we conducted structural relaxations two different ways: (1) first relax the simulation volume (but keep the cubic structure) using the ideal atomic coordinates and then relax the atomic positions producing a cubic simulation cell with local atomic distortions; (2) relax the simulations cell shape, volume, and atomic positions simultaneously. As illustrated in Fig. 1(a), these two methods provided consistent results and thus the exact methodology used is not critical for evaluating the mixing enthalpy at 0 K for the transition metal carbides. The significant deviations we do note in Fig. 1(a) are when only the atomic volume is allowed to relax, demonstrating that local atomic relaxation is important in the transition metal carbides. These results also indicate that all the group IVB and VB binary B1-structured carbides have reasonably stable structures in our DFT simulations.

Using the DFT computed mixing enthalpies for the binary carbide systems, we used a least-square fitting procedure to determine the RK parameters $L^{\alpha^*}_{M_iC-M_jC}$ at 0 K in Eq. (8). Since the RK parameters are polynomials, overfitting can produce non-physical oscillations, thus it is important to use the lowest order polynomial possible to produce the physically observed changes in the mixing enthalpy. To determine the appropriate order of the RK polynomial, we examined RK polynomials from $K = 0 \sim 3$ in Eq. (10a). The fitting residuals (σ) of the least-square fitting in the binary carbide systems are shown in Fig. 1(b). The solid bars correspond to the σ from the mixed carbides without WC, while the dashed bars are for those mixed carbides including WC. The inclusion of WC in the fitting increases the residuals significantly because B1 WC is unstable at low temperatures in DFT creating more fluctuations in the computed enthalpy of mixing. More discussion regarding how WC was included in the fitting procedures will be discussed below.

Fig. 1(b) also shows the error of the binary solutions applied to modeling the ternary, $N = 3$, quaternary, $N = 4$, and quinary, $N = 5$, solutions from our SQS simulations. These results demonstrate that there is a modest amount of error, 0.005 eV/f.u. in using only binary mixing parameters for these solutions but that the error is both acceptable and does not increase with the number of elements. This error is acceptable because it is both close to the assumed accuracy of the DFT simulations, around 0.001 eV/f.u., and because it is around the error in our fitting of the binary solutions alone. Thus, while accuracy of the solution can be improved by including higher order, *e.g.* ternary interactions, it is unlikely to affect the model results or change any of our solutions

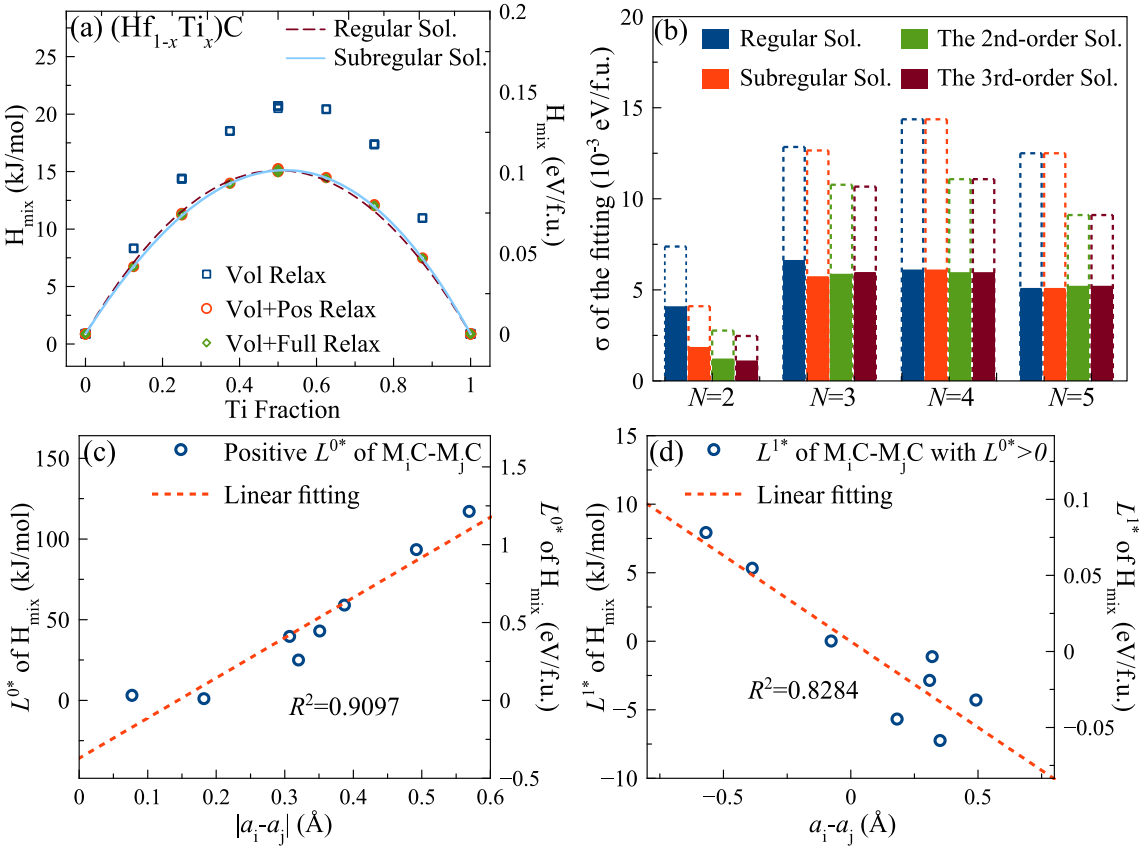

Fig. 1. The DFT results of mixing enthalpy in the pseudo-binary B1-structured carbides obtained from DFT calculations and the results of the fitted L^{α^*} parameters at 0 K. (a) $H^{\alpha^*}_{mix}$ of the pseudo-binary carbide HfC-TiC obtained from DFT at 0 K via different relaxation methods: the blue squares represent $H^{\alpha^*}_{mix}$ after the first-step volume relaxation of the SQSs; the red circles represent $H^{\alpha^*}_{mix}$ after the second-step position relaxation with the fixed volume; the green diamonds represent $H^{\alpha^*}_{mix}$ after full atomic/structural relaxation. (b) The fitting residuals (σ) of the RK polynomials for $K = 0$ (regular) to $K = 3$. The solid bars represent the σ's from the mixed carbides without WC while the dashed bars represent the σ's from the mixed carbides including WC. (c) For the pseudo-binary carbides with positive mixing enthalpy, the relationship between the $L^{\alpha 0^*}$ and lattice parameters. (d) For the pseudo-binary carbides with positive mixing enthalpy, the relationship between the $L^{\alpha 1^*}$ and lattice parameters.

substantially and we use only binary interactions for the rest of this work.

The results also demonstrate that increasing the fitting polynomial consistently decreases σ for the binary carbides ($N = 2$), but the error is not substantially reduced in high order mixtures ($N > 2$) for RK polynomials greater than a subregular solution ($K > 1$). Thus, we choose to use a subregular solution model ($K = 1$) for the mixing of all the group IVB and VB carbides in the B1 structure.

The RK polynomial values determined from fitting our DFT data are listed in Table 1. Since our model only uses the regular and subregular solution terms, the $L^{\alpha 0^*}_{M_iC-M_jC}$ and $L^{\alpha 1^*}_{M_iC-M_jC}$ terms represent the symmetric and antisymmetric part of the mixing enthalpy with respect to composition, respectively. A positive $L^{\alpha 0^*}_{M_iC-M_jC}$ value indicates that the interactions in the binary carbide system, M_iC-M_jC, tends to decrease solubility and indicates the potential for a miscibility gap; while negative values indicate the interactions favor the increased solubility. A positive $L^{\alpha 1^*}_{M_iC-M_jC}/L^{\alpha 0^*}_{M_iC-M_jC}$ ratio indicates that the $H^{\alpha^*}_{mix}$ curve tends to shift asymmetrically towards the M_iC composition while a negative value indicates the opposite. With this in mind, we can now make some general observations regarding the mixing enthalpies. The first observation is that vanadium carbide has a positive $L^{\alpha 0^*}_{M_iC-M_jC}$ parameter with all other transition metal carbides. The second observation is that the group IVB carbides have positive $L^{\alpha 0^*}_{M_iC-M_jC}$ with other group IVB carbides and negative values with the group VB carbides (that are not vanadium carbide). The above trends are consistent with the findings in the *ab-initio* study by Markström *et al.* [25] indicating a consistency amongst theoretical predictions. It is also worth comparing our results with previous experimental assessments of pseudo-binary carbide systems. Specifically, if we compare our values with those from the experiments in [24,20,21], our results reveal good consistency with the experiments with the correlation coefficients being 0.814 and -0.551 for $L^{\alpha 0^*}_{M_iC-M_jC}$ and $L^{\alpha 1^*}_{M_iC-M_jC}$ (the discrepancy comes from non-stoichiometric VC in experiments), respectively.

The small discrepancies in $L^{\alpha 0^*}_{M_iC-M_jC}$ and $L^{\alpha 1^*}_{M_iC-M_jC}$ between the *ab-initio* calculations and experiments tabulated in Table 1 may be attributed to two reasons. First, our simulation results are for stochiometric carbides where there is one carbon atom for every metal atom whereas experimental studies often result in carbon deficient, i.e. non-stoichiometric, mixed carbides [21,64]. The addition of carbon vacancies can alter the mixing enthalpy because the endpoint enthalpies of the MC_{1-x} and MC are different and the vacancies provide additional configurational entropy. Second, the mixing enthalpy from the *ab-initio* calculation was estimated at 0 K while experiments are performed at elevated temperatures.

The discrepancy between 0 K DFT simulations and experiments in Table 1 can further be seen when the DFT computed $H^{\alpha^*}_{mix}$ values are used to determine the critical temperature T^*_c for binodal phase separation, which is the minimum temperature at which there is only one single-phase B1 structure. We find that our predicted values are much higher than the experimental results [65] indicating that it is indeed important to include the temperature dependence mixing Gibbs free energy. To compute the phase diagrams of the multi-component carbides, the present work extends from these DFT calculation at 0 K to finite temperatures by taking into account the thermally induced entropy for phonons and electrons described in following section.

Previous work [15,22] has indicated that lattice constant mismatch is a potential indicator of solubility of multiple principal component alloys. This comprehensive thermodynamic assessment provides a unique opportunity to test the importance of the difference in lattice constants. To examine this outcome, we explored the pseudo-binary carbides with positive regular solution parameters ($L^{\alpha 0^*}_{M_iC-M_jC} > 0$) and found that the parameters $L^{\alpha 0^*}_{M_iC-M_jC}$ and $L^{\alpha 1^*}_{M_iC-M_jC}$ are correlated to the difference in lattice parameters of the component carbides (a_i and a_j) as illustrated in Fig. 1(c) and (d). The $L^{\alpha 0^*}_{M_iC-M_jC}$ parameters for the binary carbides exhibits a linear correlation, correlation coefficient of 0.9097, with respect to the difference in the lattice parameters $|a_i - a_j|$. This means that the mixing of the unary carbides with similar lattice parameters is favorable, which provides a physical rationale of the lattice-

Table 1

The assessment of L^{α^*} parameters in the Redlich-Kister polynomial for the B1-structured pseudo-binary carbides via both computational and experimental approaches (unit in kJ/mol). The L^{α^*} parameters assessed from experiments listed in this table are the extrapolated values at 0 K. The computed critical temperature based on $H^{\alpha^*}_{mix}$ at 0 K is labelled as T^*_c while those based on G^{α}_{mix} with the usage of the DG model is labelled as T_c (unit in K). The computed critical temperature higher than the carbide melting temperature is indicated by asterisk.

System	Present study		Assessed from Exp.		*ab-initio*[e]		Critical Temp.	
	$L^{\alpha 0^*}_{M_iC-M_jC}$	$L^{\alpha 1^*}_{M_iC-M_jC}$	$L^{\alpha 0^*}_{M_iC-M_jC}$	$L^{\alpha 1^*}_{M_iC-M_jC}$	$L^{\alpha 0^*}_{M_iC-M_jC}$	$L^{\alpha 1^*}_{M_iC-M_jC}$	T^*_c	T_c
HfC-TiC	39.12	−2.862	–	–	48.06	−7.125	2510	2048
HfC-ZrC	3.121	0.01515	–	–	–	–	<300	<300
TiC-ZrC	59.04	5.322	63.73[b]	6.000[b]	77.50	11.50	3614*	3133*
NbC-VC	42.98	−7.247	29.00[c]	−5.000[c]	65.49	−19.15	2724	1501[f]
NbC-TaC	−4.262	1.128	ideal[d]		ideal		<300	<300
TaC-VC	25.03	−11.24	48.92[a]	−0.1110[a]	36.94	−20.78	1948	1194[f]
HfC-NbC	−16.27	−5.978	15.55[a]	−0.1000[a]	−8.536	−6.327	<300	<300
HfC-TaC	−26.15	−7.989	ideal[d]		−17.13	−8.925	<300	<300
HfC-VC	93.41	−4.291	68.03[a]	43.65[a]	141.2	−20.53	5645*	2063
NbC-TiC	−24.37	5.315	–	–	−24.49	5.893	<300	<300
NbC-ZrC	−10.83	5.414	ideal[d]		ideal		<300	<300
TaC-TiC	−44.78	4.629	–	–	–	–	<300	<300
TaC-ZrC	−17.96	6.580	ideal[d]		ideal		<300	<300
TiC-VC	1.076	−5.683	–	–	12.80	−2.133	<300	<300
VC-ZrC	117.1	7.930	204.7[a]	−78.29[a]	181.4	30.73	7116*	2049

[a] Servant and Danon [24].
[b] Markström and Frisk [21].
[c] Frisk [20].
[d] Holleck [63]. Rempel and Gusev observed miscibility gap of the thin film $(NbC)_x$-$(ZrC_{0.98})_{1-x}$ at low temperatures with $L^{\alpha 0^*}_{M_iC-M_jC} = 10.15$ kJ/mol and $L^{\alpha 1^*}_{M_iC-M_jC} = 9.201$ kJ/mol [64].
[e] Markström and Frisk [25].
[f] Experimental T_c reported by Kieffer *et al.* [65]: NbC-$VC_{0.88}$ at 1740 K, TaC-$VC_{0.88}$ at 1600 K.

distortion descriptor method [15,22]. The $L^{\alpha 1*}_{M_iC-M_jC}$ parameter exhibits the negative linear correlation with respect to $a_i - a_j$ with a correlation coefficient of 0.8284. Since the $L^{\alpha 1*}_{M_iC-M_jC}$ parameter generally indicates asymmetry of the mixing enthalpy, this trend shows that it is more favorable to add a carbide with a smaller lattice parameter into the carbide with the larger lattice parameter than vice versa.

3.1.2. Phase stability at finite temperatures

To evaluate the Gibbs free energy at finite temperatures, we used the Debye-Grüneisen (DG) model as described in section 2.3. To determine the unknown λ in the model, which establishes the Grüneisen parameter, we compared the computed results using all three parameters of lambda with experimental values of the linear thermal expansion coefficients (CLE) and the heat capacity (C_p) for all the unary carbides. The result of this comparison demonstrates that a value of $\lambda = 1$ corresponds to the best agreement between our models and experiments; the full results of this analysis can be found in the *Supplemental Materials*. Thus, we used the same $\lambda = 1$ to model all the pseudo-binary carbides. The Gibbs free energies of these mixed carbides, $M_{i1-x}M_{jx}C$, were computed using the DG model which allowed us to fit the temperature-dependent parameters $L^{\alpha 0}_{M_iC-M_jC}(T)$ and $L^{\alpha 1}_{M_iC-M_jC}(T)$.

An example of this analysis is shown in Fig. 2 for the case of the $Hf_{1-x}Ti_xC$ pseudo-binary system. Fig. 2(a) is the computed Gibbs free energy as a function of temperature from the DG model using the DFT computed energy. Fig. 2(b) reveals the variation of $L^{\alpha 0}_{M_iC-M_jC}(T)$ and $L^{\alpha 1}_{M_iC-M_jC}(T)$ as a function of temperature and highlights the trends that $L^{\alpha 0}_{M_iC-M_jC}(T)$ decreases with increasing temperature while $L^{\alpha 1}_{M_iC-M_jC}(T)$ is relatively insensitive to temperature. This observed trend of $L^{\alpha 0}_{M_iC-M_jC}(T)$ is common amongst the pseudo-binary group IVB and VB transition metal carbides, which suggests that the mixing Gibbs free energy generally decreases as the temperature increases. This can be expected because all of the carbides increase their lattice parameters with increasing temperature, which would generally decrease the relative differences in lattice constants and increase solubility.

To use these results in a computational thermodynamics approach, we must have a temperature dependent parameterization of the RK polynomial coefficients. Therefore, we fit the parameters $L^{\alpha 0}_{M_iC-M_jC}(T)$ and $L^{\alpha 1}_{M_iC-M_jC}(T)$ from 0 K to 3500 K in terms of the function bases T^m and $T^n \ln T$ ($m, n \geq 2$) so that both the function basis and its first-order derivative become zero at 0 K in accordance with the third law of thermodynamics. Specifically, for our model, we choose $m = 2, 3$ and $n = 2$ which allows the coefficient of determination of the fit have an $R^2 > 0.999$ so that our functional form is:

$$L^{\alpha k}_{M_iC-M_jC}(T) = A + BT^2 + CT^3 + DT^2 \ln T. \quad (22)$$

The polynomial coefficients for $L^{\alpha 0}_{M_iC-M_jC}(T)$ and $L^{\alpha 1}_{M_iC-M_jC}(T)$ are listed in Table A3 and A4.

With the temperature dependent $L^{\alpha 0}_{M_iC-M_jC}(T)$ and $L^{\alpha 1}_{M_iC-M_jC}(T)$ functions parameterized, it is now possible to generate the pseudo-binary phase diagrams of the B1 structured group IVB and VB carbides in their solid state. Again, as an example, the phase diagrams of the HfC-TiC are shown in Fig. 2 (c) and (d). Fig. 2(c) shows the phase diagram computed using the RK polynomials formulated at 0 K, but including the entropy of mixing. Fig. 2(d) is the same phase but uses the temperature

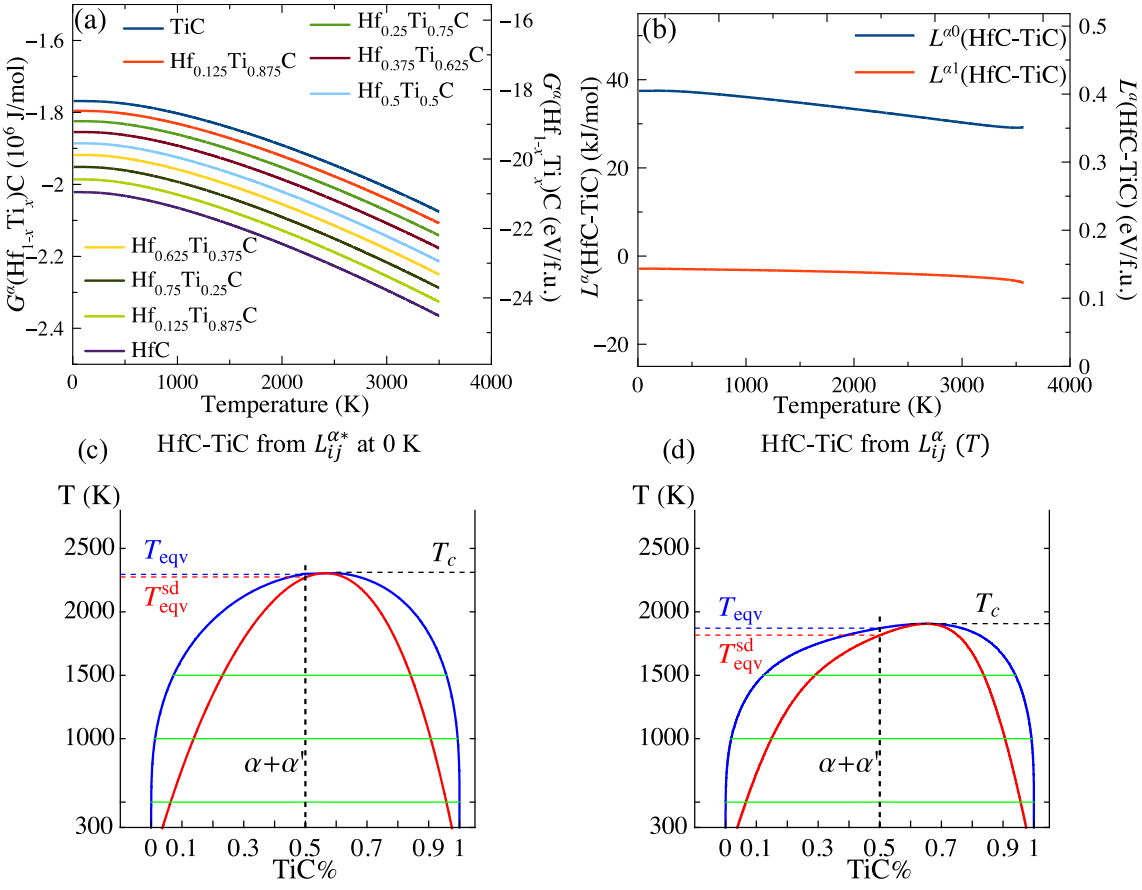

Fig. 2. (a) The estimated Gibbs free energy of $Hf_{1-x}Ti_xC$ by implementing the DG model on the DFT calculations, which include the supercells of pure TiC, HfC and the SQSs of $Hf_{1-x}Ti_xC$. (b) The fitted temperature-dependent $L^{\alpha}(T)$ parameters of $Hf_{1-x}Ti_xC$. (c) The phase diagram of the pseudo-binary $Hf_{1-x}Ti_xC$ computed from the L^{α^*} parameters at 0 K. (d) The phase diagram of the pseudo-binary $Hf_{1-x}Ti_xC$ computed from the temperature-dependent $L^{\alpha}(T)$ parameters.

Table A1
The lower temperature limit T_{eqv} for the single-phase B1-structured equiatomic multicomponent carbides. For the multicomponent carbides without WC, noted as $M_{1(1/N)}M_{2(1/N)}\cdots M_{N(1/N)}C$, T^{sd}_{eqv} represents the temperature limit for spinodal decomposition (metastable phase) while T_{eqv} represents that for the phase separation. For the multicomponent carbides including WC, noted as $M_{1[1/(N+1)]}M_{2[1/(N+1)]}\cdots M_{N[1/(N+1)]}W_{1/(N+1)}C$, values of T_{eqv}(calc.) are computed using PYCALPHAD while values of T_{eqv}(th.) are evaluated from the approximate analytical solution. For the multicomponent carbide including WC, the asterisk indicates that the mixed carbides undergo the B1-structured phase separation before the formation of a single-phase B1 structure at T^{*}_{eqv}.

Multicomponent Carbides	Without WC		Including WC	
	T^{sd}_{eqv} (K)	T_{eqv} (K)	T_{eqv}(calc.) (K)	T_{eqv}(th.) (K)
(Hf,Nb)C	<300	<300	2232	2248
(Hf,Ta)C	<300	<300	2455	2478
(Hf,Ti)C	2005	2033	1889	1895
(Hf,V)C	2041	2055	2042	2060
(Hf,Zr)C	<300	<300	1964	1966
(Nb,Ta)C	<300	<300	2365	2393
(Nb,Ti)C	<300	<300	1889	2101
(Nb,V)C	1361	1450	2042	2142
(Nb,Zr)C	<300	<300	2019	2022
(Ta,Ti)C	<300	<300	2369	2365
(Ta,V)C	1010	1132	2304	2303
(Ta,Zr)C	<300	<300	2174	2164
(Ti,V)C	<300	<300	1909	1939
(Ti,Zr)C	2880	3018	2084*	1628
(V,Zr)C	2011	2034	1826	1837
(Hf,Nb,Ta)C	<300	<300	1973	1972
(Hf,Nb,Ti)C	1432	1459	1622	1621
(Hf,Nb,V)C	1811	1864	1707	1705
(Hf,Nb,Zr)C	<300	<300	1702	1701
(Hf,Ta,Ti)C	1572	1594	1752	1751
(Hf,Ta,V)C	1876	1918	1809	1808
(Hf,Ta,Zr)C	<300	<300	1794	1793
(Hf,Ti,V)C	1931	1959	1733*	1380
(Hf,Ti,Zr)C	2277	2415	1863*	1297
(Hf,V,Zr)C	1934	2013	1851*	1451
(Nb,Ta,Ti)C	<300	<300	1865	1864
(Nb,Ta,V)C	1115	1324	1875	1874
(Nb,Ta,Zr)C	<300	<300	1834	1834
(Nb,Ti,V)C	1163	1294	1618	1617
(Nb,Ti,Zr)C	1935	1994	1499	1498
(Nb,V,Zr)C	1793	1852	1693*	1598
(Ta,Ti,V)C	1033	1244	1731	1729
(Ta,Ti,Zr)C	2083	2109	1597	1597
(Ta,V,Zr)C	1842	1884	1703*	1679
(Ti,V,Zr)C	2181	2229	1921*	1268
(Hf,Nb,Ta,Ti)C	1155	1188	1604[b]	1574[b]
(Hf,Nb,Ta,V)C	1654	1741	1646	1612
(Hf,Nb,Ta,Zr)C	<300[a]	<300[a]	1654	1624
(Hf,Nb,Ti,V)C	1695	1731	1588*	1326
(Hf,Nb,Ti,Zr)C	1759	1812	1505*	1299
(Hf,Nb,V,Zr)C	1761	1890	1738*	1383
(Hf,Ta,Ti,V)C	1709	1771	1611*	1403
(Hf,Ta,Ti,Zr)C	1873[a]	1919[a]	1528*[b]	1368[b]
(Hf,Ta,V,Zr)C	1791	1919	1751*	1444
(Hf,Ti,V,Zr)C	1990	2070	1845*	1048
(Nb,Ta,Ti,V)C	993	1286	1587[b]	1544[b]
(Nb,Ta,Ti,Zr)C	1533	1620	1523	1458
(Nb,Ta,V,Zr)C	1649	1736	1585*	1535
(Nb,Ti,V,Zr)C	1826	1874	1648*	1255
(Ta,Ti,V,Zr)C	1884	1914	1671*	1321
(Hf,Nb,Ta,Ti,V)C	1596[a]	1614[a]	1444*	1343
(Hf,Nb,Ta,Ti,Zr)C	1544[a]	1599[a]	1359*	1332
(Hf,Nb,Ta,V,Zr)C	1631	1700	1681*	1381
(Hf,Nb,Ti,V,Zr)C	1884	1896	1668*	1104
(Hf,Ta,Ti,V,Zr)C	1897	1910	1653*	1156
(Nb,Ta,Ti,V,Zr)C	1697	1728	1541*	1286
(Hf,Nb,Ta,Ti,V,Zr)C	1728	1750	1578*	1165

[a] experimentally fabricated HECs consisting of the group IVB and VB unary carbides: $(Hf_{1/4}Ta_{1/4}Ti_{1/4}Zr_{1/4})C$ [12], $(Hf_{1/4}Nb_{1/4}Ta_{1/4}Zr_{1/4})C$ [12–14], $(Hf_{1/5}Nb_{1/5}Ta_{1/5}Ti_{1/5}V_{1/5})C$ [17], $(Hf_{1/5}Nb_{1/5}Ta_{1/5}Ti_{1/5}Zr_{1/5})C$ [16,17].
[b] experimentally fabricated HECs by mixing the B1-structured unary carbides with WC: $(Hf_{1/5}Nb_{1/5}Ta_{1/5}Ti_{1/5}W_{1/5})C$, $(Hf_{1/5}Ta_{1/5}Ti_{1/5}Zr_{1/5}W_{1/5})C$, $(Nb_{1/5}Ta_{1/5}Ti_{1/5}V_{1/5}W_{1/5})C$ [17].

Table A2
The coefficients of the polynomial for the Gibbs free energy where $G(T) = A + BT^2 + CT^3 + DT^2 lnT$ (each term unit in J/mol). The E notation represents the power of 10.

Unary Carbides	A	B	C	D
HfC	−2.0189E + 6	−1.4776E-1	8.9227E-10	1.4636E-2
NbC	−1.9332E + 6	−1.1253E-1	6.8139E-7	1.0280E-2
TaC	−2.1292E + 6	−1.3623E-1	2.7557E-7	1.3195E-2
TiC	−1.7663E + 6	−7.9879E-2	1.6527E-6	5.9920E-3
VC	−1.8057E + 6	−7.1869E-2	1.7490E-6	5.0725E-3
ZrC	−1.8476E + 6	−1.2428E-1	4.5051E-7	1.1735E-2
B1 WC	−2.0692E + 6	−1.4512E-1	−9.9855E-7	1.4963E-2
B_h WC	−2.1531E + 6	−1.0861E-1	8.3923E-7	9.7788E-3

Table A3
The coefficients of the polynomial for the $L^{\alpha 0}_{M_iC-M_jC}$ (and $L^{\alpha 0}_{M_iC-WC}$) parameters in the B1-structured pseudo-binary carbides where $L^{\alpha 0}_{M_iC-M_jC}(T) = A + BT^2 + CT^3 + DT^2 \ln T$ (each term unit in J/mol). The E notation represents the power of 10.

Binary Carbides	A	B	C	D
HfC-NbC	−1.6857E + 4	−3.0538E-3	−2.6026E-7	4.7533E-4
HfC-TaC	−2.6986E + 4	2.5022E-3	−8.0195E-8	−2.4738E-4
HfC-TiC	3.7586E + 4	−4.8640E-3	6.1856E-8	4.8395E-4
HfC-VC	8.7226E + 4	−5.0705E-2	−1.5625E-6	5.3936E-3
HfC-ZrC	3.0959E + 3	−7.8256E-3	−5.7700E-7	1.0845E-3
NbC-TaC	−5.4731E + 3	−1.1986E-2	−2.1747E-7	1.3411E-3
NbC-TiC	−2.5284E + 4	6.3457E-3	2.0958E-7	−7.6988E-4
NbC-VC	3.9110E + 4	−5.3651E-2	−3.0737E-6	6.7795E-3
NbC-ZrC	−1.1509E + 4	−1.2124E-2	−9.301E-7	1.6855E-3
TaC-TiC	−4.6312E + 4	1.1270E-2	4.1877E-7	−1.4068E-3
TaC-VC	2.1567E + 4	−3.6935E-2	−2.3242E-6	4.9993E-3
TaC-ZrC	−1.8865E + 4	−1.2449E-2	−8.3662E-7	1.7246E-3
TiC-VC	5.9107E + 2	−1.3429E-2	−1.5376E-6	2.4525E-3
TiC-ZrC	5.7683E + 4	−1.6098E-2	−6.6954E-7	2.1146E-3
VC-ZrC	1.0849E + 5	−4.0669E-2	3.3709E-6	2.0164E-3
HfC-WC	−5.7733E + 4	−6.6100E-2	−6.4829E-7	6.7232E-3
NbC-WC	−2.0853E + 4	−8.2475E-2	−1.7500E-6	8.0858E-3
TaC-WC	−2.1531E + 4	−7.1890E-2	−5.8879E-7	7.2891E-3
TiC-WC	−1.0872E + 5	−1.7103E-2	1.7646E-6	2.4416E-4
VC-WC	−4.2340E + 4	−4.2139E-2	6.9157E-7	2.4416E-3
ZrC-WC	−4.9997E + 4	−1.1014E-1	−4.6254E-6	1.1916E-2

Table A4
The coefficients of the polynomial for the $L^{\alpha 1}_{M_iC-M_jC}(T)$ parameters in the B1-structured pseudo-binary carbides where $L^{\alpha 1}_{M_iC-M_jC}(T) = A + BT^2 + CT^3 + DT^2 \ln T$ (each term unit in J/mol). The E notation represents the power of 10.

Binary Carbides	A	B	C	D
HfC-NbC	−5.3802E + 3	9.8886E-3	8.0215E-7	−1.3614E-3
HfC-TaC	−6.6560E + 3	−7.8172E-3	3.8528E-7	8.1063E-4
HfC-TiC	−2.8180E + 3	−3.6496E-3	−2.0207E-7	5.0669E-4
HfC-VC	−2.9730E + 3	−2.3109E-2	−4.8067E-6	4.2747E-3
HfC-ZrC	1.7527E + 2	−8.1767E-3	1.7053E-7	8.2711E-4
NbC-TaC	1.1097E + 3	1.0519E-2	−5.7160E-7	−1.1883E-3
NbC-TiC	4.7680E + 3	−6.0899E-3	−2.4839E-7	4.1316E-4
NbC-VC	−7.2304E + 3	8.0358E-3	1.5375E-6	−1.4873E-3
NbC-ZrC	4.6764E + 3	−1.2518E-2	−1.1005E-6	1.5979E-3
TaC-TiC	3.4786E + 3	−2.9670E-3	−6.8538E-7	3.0019E-4
TaC-VC	−9.8536E + 3	3.8904E-2	2.8358E-6	−5.6659E-3
TaC-ZrC	5.1234E + 3	1.4594E-2	2.7520E-7	−2.0510E-3
TiC-VC	−4.4717E + 3	2.8586E-2	1.9385E-6	−4.0210E-3
TiC-ZrC	5.5473E + 3	−5.218E-3	−1.1953E-7	4.6884E-4
VC-ZrC	8.0877E + 3	3.5176E-2	6.2459E-6	−6.3341E-3

dependent RK polynomials and thus the temperature dependent Gibbs free energy of mixing. The inclusion of the temperature dependent Gibbs free energy of mixing causes the critical temperature to decrease. For clarity, the critical temperatures for the pseudo-binary carbides evaluated using the RK polynomials evaluated at 0 K (T_c^*) and those evaluated at finite temperatures (T_c) are tabulated in Table 1. If we compare our computed critical temperatures with experimental reports of the NbC-$VC_{0.88}$ and TaC-$VC_{0.88}$ systems (in Table 1), we find the computed T_c using the temperature dependent $L^{\alpha}(T)$ parameters are modestly lower than the experimental values but still show a good agreement. The underestimation of T_c in this study via our computational approach can be attributed to the carbon vacancies in $VC_{0.88}$ which lowers the Gibbs free energy relative to the stoichiometric VC used in our model, thus raising the critical temperature. While we could use $VC_{0.88}$ in our pseudo-binary simulations, the aim of this work is the evaluation of the multicomponent carbides which are all nearly equal metal and carbon atoms facilitating the need to use stoichiometric VC. With these comparisons, we can conclude that our DG model is reasonable for the evaluation of the temperature dependent $L^{\alpha}(T)$ parameters and the phase diagrams of the pseudo-multicomponent carbides can be reasonably computed with these parameters (see Table A2–A4).

With this established, we can now examine the ability to mix equiatomic transition metals in multicomponent principal elements carbides, i.e. HECs. We now turn our attention to the temperatures for mixing the carbides as T_{eqv}^{sd} and T_{eqv}. As shown in Fig. 2(d), the red curve (spinodal) and blue curve (binodal) represent the limits of spinodal decomposition and the miscibility gap, respectively. Thus, T_{eqv}^{sd} and T_{eqv} can be determined from value of these curves at a composition of 50 mol %, *e.g.* $Hf_{0.5}Ti_{0.5}C$, as shown in Fig. 2(c)-(d). T_{eqv} represents the lower temperature limit for the equilibrium of the single-phase $Hf_{0.5}Ti_{0.5}C$ phase while T_{eqv}^{sd} can be regarded as the lowest temperature for the existence of the single-phase $Hf_{0.5}Ti_{0.5}C$ since the region below this curve should undergo spinodal decomposition. This analysis provides two estimates for the temperature limits of the stability of equiatomic pseudo-binary carbide systems.

The same approach can be used to compute T_{eqv}^{sd} and T_{eqv} in the pseudo-ternary and greater carbide solutions. As another example, the pseudo-ternary system HfC-TiC-ZrC was evaluated using the temperature dependent RK coefficients and is plotted in Fig. 3. Since the ZrC-TiC system has the largest value of $L_{M_iC-M_jC}^{\alpha 0*}$, this is the last miscibility gap that forms, which is highlighted in Fig. 3 at the two temperatures where T_{eqv}^{sd} and T_{eqv} are determined. This approach was used on all possible combinations of the group IVB and VB transition metal carbides from pseudo-binary to pseudo-senary solutions and the collective results of the temperature limits for the single-phase equiatomic multicomponent carbides are listed in Table A1.

Several trends can be observed from the results in Table A1 regarding mixing of the B1 structured transition metal carbides. First, TiC-ZrC has the largest excess mixing Gibbs free energy G_{mix}^{α}, as evidenced by its highest T_c in Table 1. This results in high T_c values for all mixed carbides that contain Ti and Zr. Second, the mixing entropy, S_{mix}, plays an important role by generally lowering the temperature limits for the single-phase mixed carbides. For example, the T_{eqv} for the pseudo-binary carbide $Ti_{0.5}Zr_{0.5}C$ is 3018 K, which is lowered to 1750 K for the pseudo-senary carbide $(Hf_{1/6}Nb_{1/6}Ta_{1/6}Ti_{1/6}V_{1/6}Zr_{1/6})C$. However, the mixing entropy is not sufficiently large as to offset the excess mixing enthalpy at room temperature, which means most of the mixed carbides with positive $L_{M_iC-M_jC}^{\alpha 0*}$ parameters are not in a single-phase B1 structure at 300 K. Another observation worth pointing out is that the inclusion of more transition metals does not universally lower T_{eqv}. For example, the HfC-NbC-TiC pseudo-ternary carbide has a $T_{eqv} = 1432$ K and, if Zr is added to the mixture, $T_{eqv} = 1759$ K for the pseudo-quaternary carbide. Therefore, even at relatively high temperatures the excess mixing enthalpy is as important as entropy which suggests the formation of these solutions is not dominated by entropy.

Among those experimentally synthesized HECs, our computational study reveals that one of these reported carbides, $(Hf_{1/4}Nb_{1/4}Ta_{1/4}Zr_{1/4})C$ [12–14], should form a single-phase B1 structure at room temperature because the system has negative excess mixing enthalpy, while the other reported single-phase carbides, i.e. $(Hf_{1/4}Nb_{1/4}Ti_{1/4}Zr_{1/4})C$ [12], $(Hf_{1/5}Nb_{1/5}Ta_{1/5}Ti_{1/5}V_{1/5})C$ [17], and $(Hf_{1/5}Nb_{1/5}Ta_{1/5}Ti_{1/5}Zr_{1/5})C$ [16,17], are not thermodynamically stable at room temperature. We are aware that the mixed carbides in this study are assumed to be stoichiometric with no carbon vacancies and that the non-stoichiometric mixed carbides may have a lower excess mixing energy and a higher configurational entropy because of the presence of vacancies. Nevertheless, it is unlikely that vacancy contributions to the total energy state would lower the T_{eqv} by about the 1000 K necessary to form a single-phase HECs at room temperature. In summary, the single-phase HECs that are stable at room temperature can be attributed to the negative excess mixing enthalpy instead of the configurational mixing entropy and that even at high temperatures, the two often compete to determine phase stability. These observations call into question the use of the term 'high entropy carbides' used extensively in the literature.

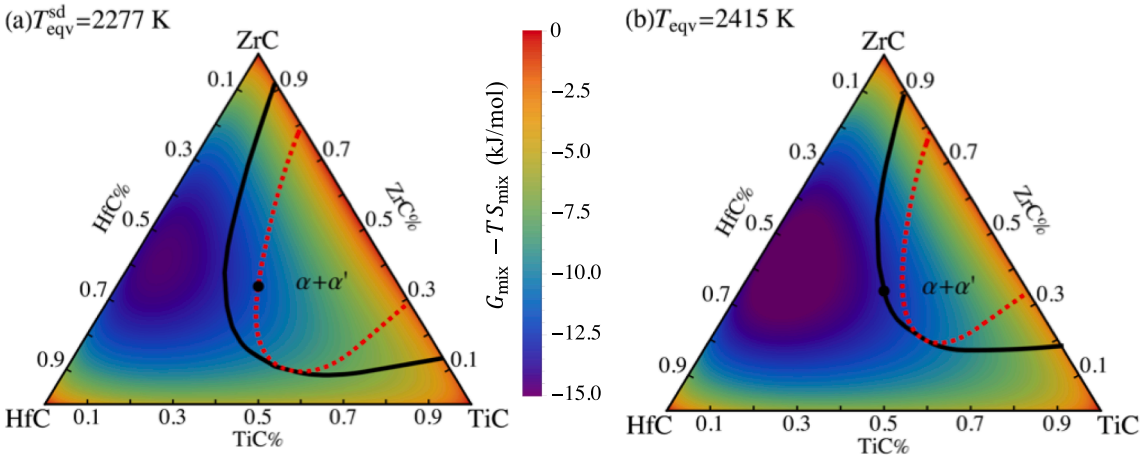

Fig. 3. The phase diagram of the pseudo-ternary carbide HfC-TiC-ZrC. (a) At $T_{eqv}^{sd} = 2277$ K, the equiatomic mixed carbide $(Hf_{1/3}Ti_{1/3}Zr_{1/3})C$ is on the boundary of the spinodal decomposition region. (b) At $T_{eqv} = 2415$ K, the equiatomic mixed carbide $(Hf_{1/3}Ti_{1/3}Zr_{1/3})C$ is on the binodal line. The colour bar indicates the total excess mixing free energy.

3.2. Mixing of the B1-structured unary carbides with WC

As noted in the introduction, there have been efforts of including tungsten as a principal element in the HECs even though it does not typically form the B1 structure. Thus, it is important to understand how the inclusion of a group VIB elements affects the phase stability of the B1-structured HECs.

3.2.1. Ab-initio assessment at 0 K

In order to account for W in the B1-structured HECs, we have to include both the excess mixing Gibbs free energy of tungsten in the B1 structure as well as for the B_h structure, which would thermodynamically compete with the B1 structure. We first started with our model for the excess mixing Gibbs free energy of the B_h structure. As mentioned previously, we modeled the group IVB and VB transition metals as point defects in the B_h structure since the B_h $M_{1-x}W_xC$ SQS supercells deformed excessively (into a rhombohedral structure) for $x \leq 7/8$, thus we could not construct an accurate set of RK polynomials. To obtain the excess enthalpy, $\Delta H^{\beta^*}_{M_iC}$ of a metal carbide point defect, a convergence study was performed with regards to the DFT supercell size that included 16, 32, 54, 64, 96, 128, 160, and 250 atoms. Fig. 4(c) shows that $\Delta H^{\beta^*}_{M_iC}$ converges within ±0.02 eV/f.u. for a supercell with 128 atoms or more with generally weak size dependence above 54 atoms. This suggests that our model should be reasonably accurate for solute atomic fractions of up to 2%. Fig. 4(c) also demonstrates that the excess energy $\Delta H^{\beta^*}_{M_iC}$ of a group IVB point-defect in B_h WC is higher than that of a group VB point-defect carbide. This trend can be understood in terms of the differences in the cohesive energies between the B1 and B_h phases in the TMCs, which decreases with increasing number of valence electrons [66].

When attempting to evaluate the RK polynomials of the pseudo-binary solutions with tungsten at 0 K for the B1 structure, we found a similar issue as with the B_h structure. As the molar fraction of WC increased, the structure deformed more although the distortions were not as severe as occurred in the B_h structure. Fig. 4(a) shows the mixing enthalpy computed using our SQSs for two specific $M_{1-x}W_xC$ solutions, $Hf_{1-x}W_xC$ and $Ta_{1-x}W_xC$, since they have the same inner shell electrons and only differ in their valency. These two curves illustrate the general trends of the mixing enthalpy at 0 K (H^*_{mix}), which is to significantly curve towards the B1-WC. To quantify the distortion of $M_{1-x}W_xC$ solution from the cubic structure, we computed the Green-Lagrange strain (ε) of the relaxed structure and the 2-norm of ε is plotted in Fig. 4(b). These results confirm that the distortion of the B1-structured $M_{1-x}W_xC$ solution increases as the WC composition increases. If we compare the distortions with those of a B1 pseudo-binary solution, *e.g.* $Hf_{1-x}Ta_xC$, we can see that a typical B1 pseudo-binary solution typically maximizes the strain at (or near) the equiatomic composition and the strains decrease towards zero at the end compositions. However, for solutions containing WC, the strains do not go back to zero near stoichiometric WC; they actually get larger as this composition is approached. The strains only trend back to zero at this composition because the B1 WC is constrained not to deform by the DFT supercell; recall that B1 WC is dynamically unstable at 0 K but can be confined to the B1 structure by symmetry. Consequently, as illustrated in Fig. 1(b), large fitting residuals are found for the fitted L parameters if all DFT results of the B1-structured $M_{1-x}W_xC$ are included. This indicates that the supercells with high tungsten concentration are largely distorted and should be excluded from our fitting procedure as they are no longer representative of a B1 solution. To

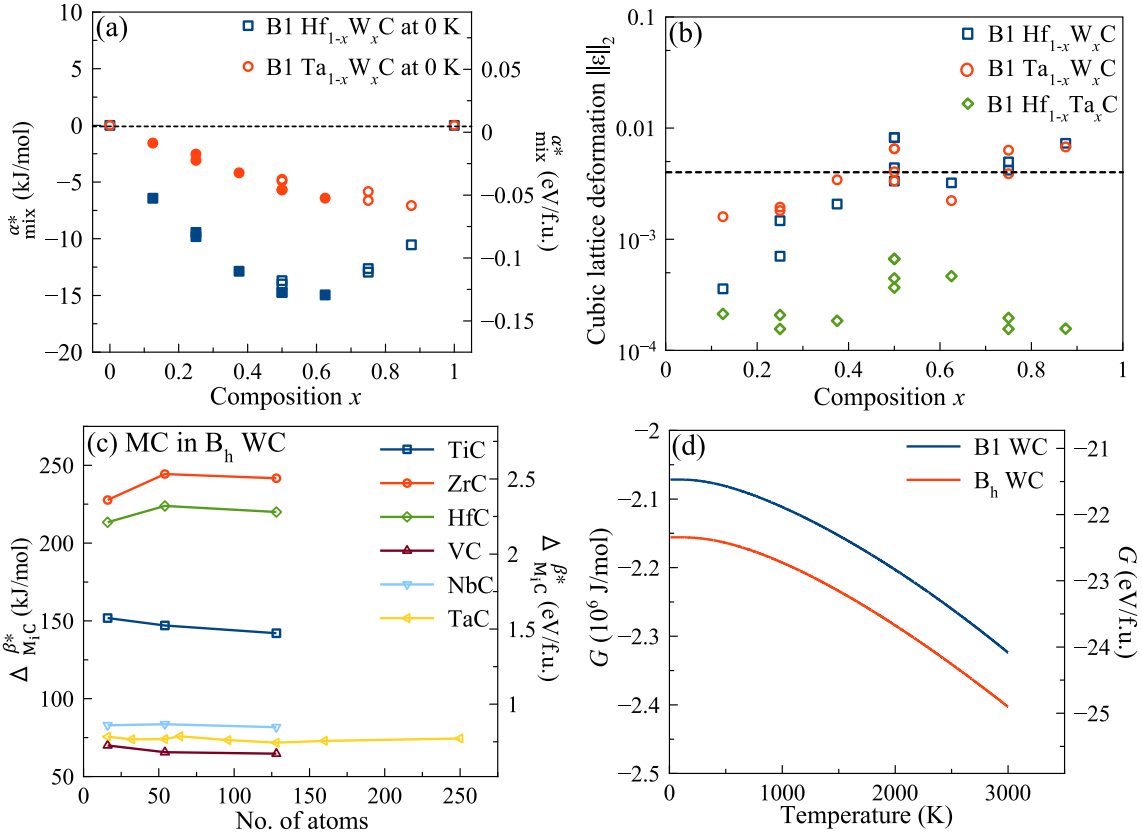

Fig. 4. (a) The mixing enthalpy of the B1-structured pseudo-binary carbides $Hf_{1-x}W_xC$ and $Ta_{1-x}W_xC$ obtained in the DFT simulation where the solid points stand for the selected data to fit the $L^{\alpha^*}_{M_iC-WC}$ parameters. (b) The deformation of the SQSs of the B1-structured pseudo-binary carbides after the full relaxation DFT simulation where the blue region represents the cut-off deformation $\|\varepsilon\|_2$. (c) The convergence of the excess energy of the point-defect carbides inside the B_h WC with respect to the size of the simulated supercell. (d) The computed Gibbs free energy of both the B1-structured (G^{α}_{WC}) and B_h-structured WC (G^{β}_{WC}) by using the DFT simulation and the DG model.

provide a rationale way to exclude DFT data from our fitting procedure, a distortion cutoff was used to restrict the DFT data used in our fitting of the $M_{1-x}W_xC$ solutions. Based on the distortions in the pseudo-binary carbides consisting of only B1-structured unary carbides, a distortion cutoff was chosen as $\|\varepsilon\|_2 \leq 4.0 \times 10^{-3}$, which is the largest distortion among the B1-structured binary carbides (specifically, $Ta_{0.5}V_{0.5}C$). As illustrated in Fig. 4(b), the DFT data of $Hf_{1-x}W_xC$ and $Ta_{1-x}W_xC$ with $\|\varepsilon\|_2 \leq 4.0 \times 10^{-3}$ (in blue region) are used to fit the L parameters. This results in the exclusion all data that has greater than 62.5 mol % tungsten, *e.g.* $M_{1-x}W_xC$ with $x > 0.625$, and thus we only use a regular solution to model WC interactions with other transition metals in the B1 structure and only $L^{0*}_{M_iC-WC}$ terms are reported. The results of the fitting demonstrate that $L^{0*}_{M_iC-WC} < 0$ with $Ta_{1-x}W_xC$ and $Hf_{1-x}W_xC$ taken as examples and are shown in Fig. 4(a). However, the negative values in this case do not indicate that WC will readily dissolve into the B1 structure. Since the B_h WC is the stable structure for WC instead of B1 WC, the phase equilibrium between the B1 structure and B_h structure should be factored in when considering the stabilization of WC in a B1-structured HECs, which is elaborated upon in the following sections.

3.2.2. Analytical solution of the phase-equilibrium equiatomic mixed carbides

Determining the temperature at which tungsten carbide can be mixed into a B1-structured solution is a challenging problem because of the large number of elements (up to 7) and the two different structures involved (B1 and B_h) as well as the potential for spinodal decomposition. However, phase equilibrium, Eq. (4), can be reduced into two independent PDEs by making two assumptions. First, G^α only has only one local minimum near the equiatomic composition at temperature T, and second, the B_h-structured mixed carbide has low concentrations of the group IVB and VB elements ($x^\beta_W \approx 1$). In this case, there are only two variables (x^α_W,x^β_W) and the Gibbs free energy for $(M_{1x_1}M_{2x_2}\cdots M_{Nx_N}W_{x_W})C$ reduces to:

$$G^\alpha = x^\alpha_W G^\alpha_{WC} + \left(1-x^\alpha_W\right)\overline{G}^\alpha_{MC} + G^\alpha_{mix} + k_BT\left[x^\alpha_W \ln x^\alpha_W + \left(1-x^\alpha_W\right)\ln\left(\frac{1-x^\alpha_W}{N}\right)\right], \tag{23}$$

$$G^\beta = x^\beta_W G^\beta_{WC} + \left(1-x^\beta_W\right)\left(\overline{G}^\alpha_{MC} + \Delta\overline{G}^\beta_{MC}\right) + k_BT\left[x^\alpha_W \ln x^\beta_W + \left(1-x^\beta_W\right)\ln\left(\frac{1-x^\beta_W}{N}\right)\right]. \tag{24}$$

where α and β represent the B1 and B_h phases, respectively. In Eqs. (23) and (24), $\overline{G}^\alpha_{MC} = \sum_{i=1}^N G^\alpha_{M_iC}/N$ is the average Gibbs free energy of the B1-structured carbide (excluding WC) and $\Delta\overline{G}^\beta_{MC} = \sum_{i=1}^N \Delta G^\beta_{M_iC}/N$ is the average excess energy of the point-defects inside the B_h phase.

In this study, the goal is to determine the lower temperature limit T_{eqv} for the B1-structured equiatomic mixed carbides and thus the compositions in the B1 structure are known. By substituting $x^\alpha_W = 1/(N+1)$ into Eqs. (23) and (24), the approximate T_{eqv} has the following analytical form:

$$\gamma = \frac{\Delta\overline{G}^\beta_{MC} - \overline{L}^{\alpha 0}_{M_iC-WC}/(N+1)^2 - (N-1)(N+2)\overline{L}^{\alpha 0}_{M_iC-M_jC}/[2(N+1)^2]}{\left(G^\alpha_{WC} - G^\beta_{WC}\right) + N^2\overline{L}^{\alpha 0}_{M_iC-WC}/(N+1)^2 - (N-1)N\overline{L}^{\alpha 0}_{M_iC-M_jC}/[2(N+1)^2]}, \tag{25}$$

$$\tau = (1+\gamma)^{1/\gamma} - \frac{1}{\gamma}, \tag{26}$$

$$k_BT_{eqv} = \frac{\left(G^\alpha_{WC} - G^\beta_{WC}\right) + N^2\overline{L}^{\alpha 0}_{M_iC-WC}/(N+1)^2 - (N-1)N\overline{L}^{\alpha 0}_{M_iC-M_jC}/[2(N+1)^2]}{\ln(N+1) + \ln[1-(N+\tau)^{-\gamma}]}. \tag{27}$$

In the above equations, the term $\overline{L}^{\alpha 0}_{M_iC-WC}$ is the average $L^{\alpha 0}$ parameters for the B1-structured pseudo-binary carbides with tungsten, i.e. M_iC-WC, where M_iC represents the group IVB and VB carbides. Likewise, the term $\overline{L}^{\alpha 0}_{M_iC-M_jC}$ represents the average $L^{\alpha 0}$ parameters for the B1-structured pseudo-binary carbides M_iC-M_jC. These expressions are shown in Eq. (28) below.

$$\overline{L}^{\alpha 0}_{M_iC-WC} = \frac{1}{N}\sum_{i=1}^N L^{\alpha 0}_{M_iC-WC}, \overline{L}^{\alpha 0}_{M_iC-M_jC} = \frac{2}{N(N-1)}\sum_{i=1,j>i}^N L^{\alpha 0}_{M_iC-M_jC}. \tag{28}$$

The parameter γ in Eq. (25) governs the stability of the solution and the derivation details for T_{eqv} are covered in the *Supplemental Materials*. According to Eq. (27), the term $\ln(N+1)$ is the leading term in the denominator, which means the mixing configurational entropy increases as the number of carbide components increases thus significantly lowering T_{eqv}.

The leading terms in the numerator in Eq. (27) are $\left(G^\alpha_{WC} - G^\beta_{WC}\right)$, $\overline{L}^{\alpha 0}_{M_iC-WC}$ and $\overline{L}^{\alpha 0}_{M_iC-M_jC}$. The first term is not influenced by which elements are used to dissolve WC in the B1 structure since it is just the Gibbs free energy difference between B1 WC and B_h WC. It is also weakly temperature dependent and ranges in values from 0.82 ~ 0.87 eV/f.u. between 0 K and 3000 K as illustrated in Fig. 4(d). The second term indicates that the lower values of $\overline{L}^{\alpha 0}_{M_iC-WC}$ results in a lower T_{eqv}, which suggests that it is best to select group IVB and VB transition metals that have smaller (or more negative) values of $L^{\alpha 0}_{M_iC-WC}$ to improve solubility. This is an obvious result but further indicates that WC will be more soluble in the group IVB carbides than the group VB carbides because of the trends that the $L^{\alpha 0}_{M_iC-WC}$ values follow for the group IVB carbides, *i.e.*, they are generally smaller (or more negative) than those for the group VB carbides. Finally, the $\overline{L}^{\alpha 0}_{M_iC-M_jC}$ terms suggest that T_{eqv} can be lowered by choosing the B1 carbides to be less soluble together, as this raises the Gibbs free energy of the B1 solution making it easier to dissolve WC in it. However, it is critical that the three aforementioned terms are interdependent and thus not independently controllable. The term $\Delta\overline{G}^\beta_{MC}$ in Eq. (25), which is the average defect formation energy in the B_h structure, only contribute to γ directly, thus has the minimal effect on T_{eqv}. The $\Delta G^\beta_{MC}/\left(G^\alpha_{WC} - G^\beta_{WC}\right)$ ranges between 1 ~ 3 only resulting in a 20 K difference in T_{eqv}. The effects of the three terms - N, $\overline{L}^{\alpha 0}_{M_iC-M_jC}$, and $\overline{L}^{\alpha 0}_{M_iC-WC}$ - on T_{eqv} are illustrated in Fig. 5 by choosing $\left(G^\alpha_{WC} - G^\beta_{WC}\right) = 0.85$ eV/f.u. and $\Delta G^\beta_{MC}/\left(G^\alpha_{WC} - G^\beta_{WC}\right) = 2$.

To provide a more thorough understanding of the predictions of the analytical model, we choose to plot T_{eqv} as a function of $\overline{L}^{\alpha 0}_{M_iC-M_jC}$, $\overline{L}^{\alpha 0}_{M_iC-WC}$ for different N values in Fig. 5. First, it is clear from these plots that $\gamma \geq 1/N$ for T_{eqv} to exist, which is embodies the assumptions that enable the analytical solution. Specifically, the analytical solution does not exist when the term $\overline{L}^{\alpha 0}_{M_iC-M_jC}$ or $\overline{L}^{\alpha 0}_{M_iC-WC}$ is a large positive number, which indicates G^α likely has multiple local minimums or the concentrations of the group IVB and VB carbides in the B_h-structured mixed carbide are not negligible. It is worth noting that the conditions for the existence of the analytical solution are not always met for the mixed carbides, especially when they contain a large number of mixed carbides.

The results in Fig. 5 also confirm that, in general, smaller (more negative) $\overline{L}^{\alpha 0}_{M_iC-WC}$, larger (more positive) $\overline{L}^{\alpha 0}_{M_iC-WC}$, and larger N all lead to a lower T_{eqv}. However, to make $T_{eqv} \leq 300$ K, all three terms (N, $\overline{L}^{\alpha 0}_{M_iC-M_jC}$ and $\overline{L}^{\alpha 0}_{M_iC-WC}$) must be chosen to make the numerator in Eq. (27) a small, positive value. However, in the real transition metal carbides these three terms are not independent and, in fact, no combination of the 7 transition metal carbides studied here, using our analytical model, results in a $T_{eqv} \leq 300$ K. This conclusion is further supported by our

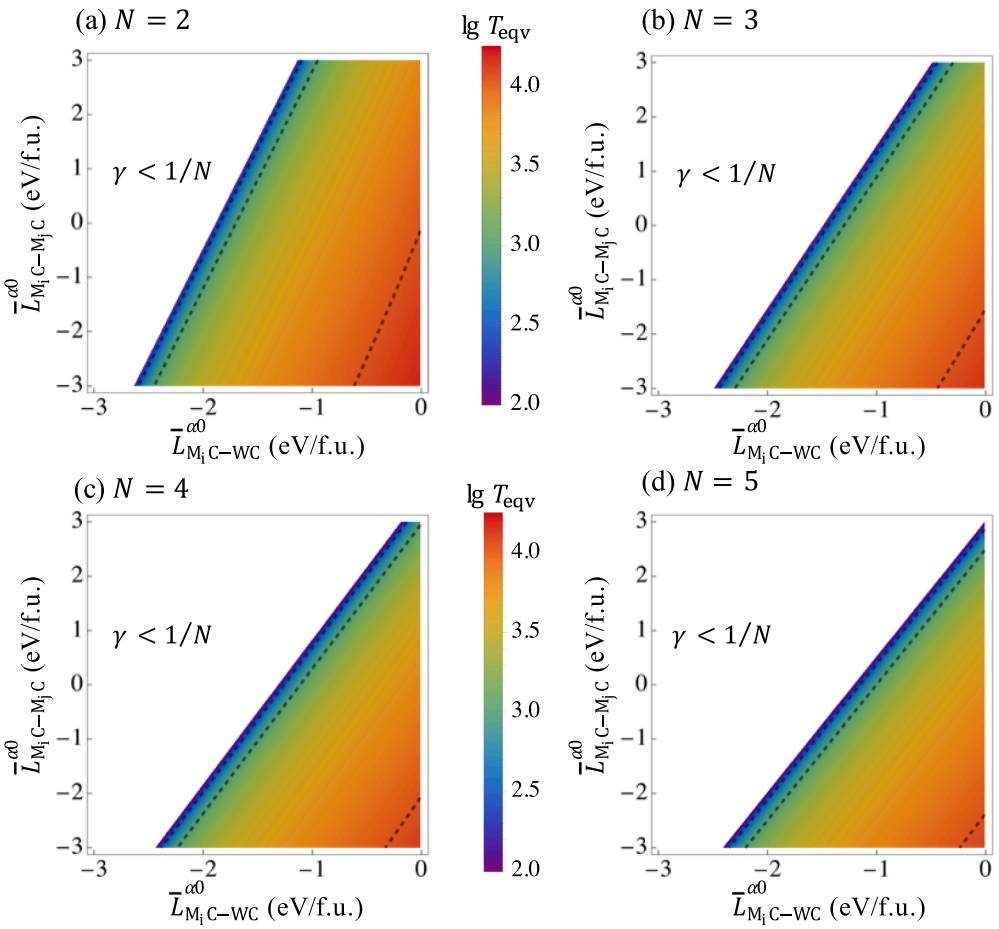

Fig. 5. The effects of N, $\bar{L}^{\alpha 0}_{M_iC-M_jC}$ and $\bar{L}^{\alpha 0}_{M_iC-WC}$ in T_{eqv} where the contours represent $T_{eqv} = 10^{2.5} \cong 325$ K, $T_{eqv} = 10^3$ K, and $T_{eqv} = 10^4$ K.

numerical solutions to the exact phase equilibrium equations discussed below.

3.2.3. Phase stability at finite temperatures

In order to compute T_{eqv}, it is first necessary to compute the temperature dependent parameters $\Delta G^{\beta}_{M_iC}$ and $L^{0\alpha}_{M_iC-WC}$, associated with the terms $\Delta H^{\beta *}_{M_iC}$ and $L^{0\alpha *}_{M_iC-WC}$ evaluated at 0 K using DFT. This was done again using the DG model to evaluate the Gibbs free energy at finite temperature and then extracting the necessary values, which are plotted in Fig. 6. The trends of the $L^{0\alpha}_{M_iC-WC}$ parameters as a function of temperature suggest that the B1-structured WC becomes more soluble with other B1-structured carbides as temperature increases, which is as expected because of the lattice thermal expansion. The $\Delta G^{\beta}_{M_iC}$ term, which represents the defect formation energy of the metal carbide in B_h tungsten carbide, changes more dramatically with temperature for the group IVB carbides as compared with the group VB carbides, which is likely a result of the more directional bonds in the group IVB carbides [67] (see Table A5).

The lower temperature limits T_{eqv} for the B1-structured equiatomic multicomponent carbides are evaluated two different ways: calculated using PYCALPHAD and estimated from the analytical solution, noted as T_{eqv}(calc.) and T_{eqv}(th.), respectively. For the pseudo-binary carbides ($N = 1$), the analytical solution T_{eqv}(th.) is the exact solution and coincides with the numerical value T_{eqv}(calc.). However, most of the T_{eqv} s for the single-phase $M_{i0.5}W_{0.5}C$ are higher than the melting temperature of B_h WC, as shown in the phase diagrams for $M_{i1-x}W_xC$ in the *Supplemental Materials*. For $N \geq 2$, the collective results of T_{eqv}(calc.) and T_{eqv}(th.) are listed in Table A1. The calculated results can be broken up into two cases. In the first case, the M_iC and M_jC in the mixed carbides have a negative, $\bar{L}^{\alpha 0}_{M_iC-M_jC} < 0$ or a small positive excess mixing enthalpy ($\bar{L}^{\alpha 0}_{M_iC-M_jC} \ll k_B T \ln N$). At T_{eqv}(calc.), phase equilibrium is reached between the single B1-structured phase (α) and the single B_h-structured phase (β). This case meets the assumptions of the analytical solution and the temperatures computed using both methods are in good agreement. In the second case, the mixed carbide includes several components with large positive $L^{0\alpha}_{M_iC-M_jC}$ parameters and thus a large positive $\bar{L}^{\alpha 0}_{M_iC-M_jC}$. In this case, the phase separation of the single B1 structure into two B1 phases must be taken into account since it is often the limiting temperature. This violates the assumptions of the analytical solution, and therefore the analytical solution predicts a T_{eqv}(th.) that is too low. The phase diagrams of the pseudo-ternary carbides, HfC-ZrC-WC and TiC-ZrC-WC, are plotted in Fig. 6 as the examples of these two cases.

While the analytical model is useful in describing how the parameter might affect T_{eqv}, it is still instructive to discuss the trends observed using the actual data from the DFT-DG model. From Table A1, we can observe a few overall trends. First and foremost, the data in Table A1 demonstrates that it is not possible to form a single-phase B1 structured equiatomic HEC with WC at room temperature; they should only be thermodynamically stable at temperatures above 1000 K. Even though increasing the number of elements helps decrease T_{eqv}, the enthalpy of mixing as described by $\bar{L}^{\alpha 0}_{M_iC-M_jC}$ and $\bar{L}^{\alpha 0}_{M_iC-WC}$ are equally important. This is particularly noteworthy because as the number of elements in the mixture are increased, the more elements are added that do not wish to mix, *i.e.*, they have a large positive mixing enthalpy with such example mixtures being HfC-VC, HfC-TiC, NbC-VC, TaC-VC, TiC-ZrC and VC-ZrC. For these mixed carbides, their T_{eqv} s are relatively high because of the

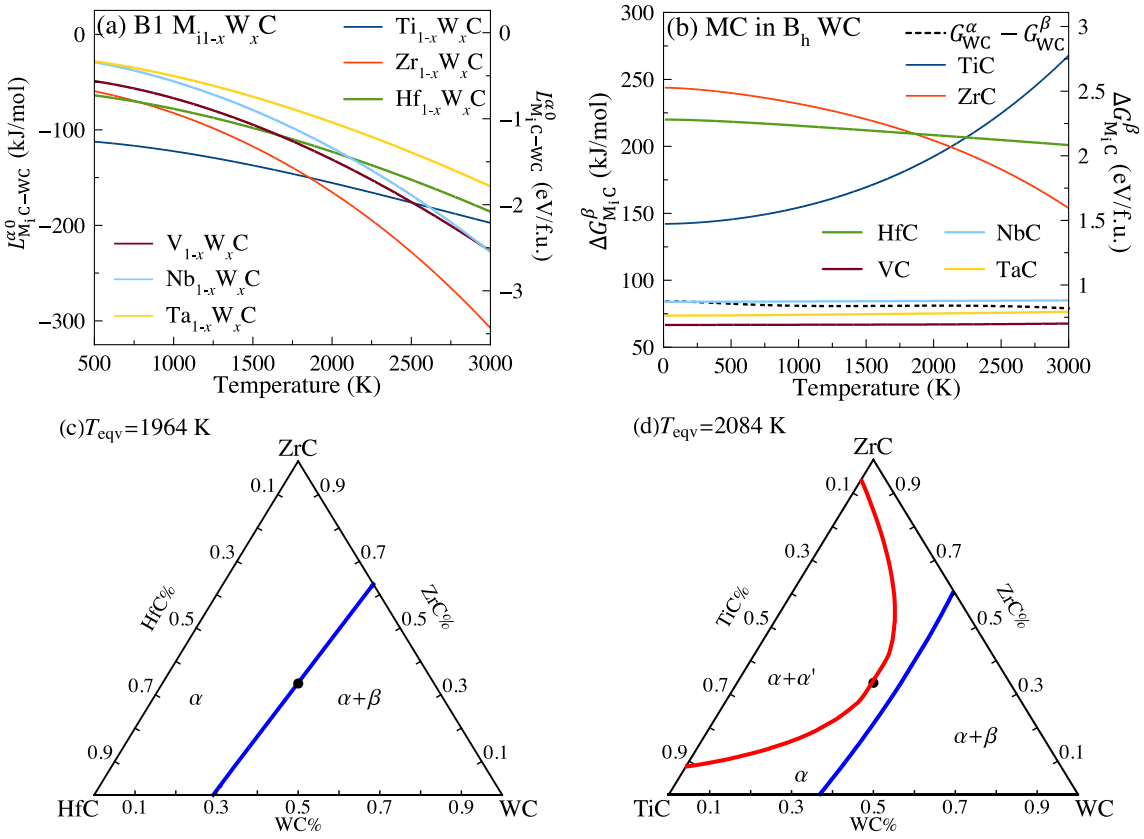

Fig. 6. (a) the temperature dependent $\bar{L}^{\alpha 0}_{M_iC-WC}$ parameters for the B1-structured pseudo-binary carbides $M_{i1-x}W_xC$ where M_iC represents the group IVB and VB carbides; (b) the temperature dependent $\Delta G^{\beta}_{M_iC}$ for the point-defect M_iC inside the B_h WC; (c) the phase diagram for the pseudo-ternary carbide HfC-ZrC-WC where the black dot represents the equiatomic composition; (d) the phase diagram for the pseudo-ternary carbide TiC-ZrC-WC where the black dot represents the equiatomic composition.

Table A5
The coefficients of the polynomial for the Gibbs free energy $\Delta G^{\beta}_{M_iC}(T)$ when the B1-structured carbides M_iC are doped into the B_h WC as point defects, where $\Delta G^{\beta}_{M_iC}(T) = A + BT^2 + CT^3 + DT^2\ln T$ (each term unit in J/mol). The E notation represents the power of 10.

B_h-WC Substrate	A	B	C	D
HfC in B_h WC	2.2002E + 5	−2.6529E-2	−5.3346E-7	3.2489E-3
NbC in B_h WC	8.3924E + 4	2.0746E-3	6.4389E-8	−2.6852E-4
TaC in B_h WC	7.3627E + 4	3.6739E-3	1.0941E-7	−4.6006E-4
TiC in B_h WC	1.4213E + 5	3.4239E-2	2.8708E-6	−3.6069E-3
VC in B_h WC	6.6661E + 4	1.8591E-3	1.3295E-7	−2.6746E-4
ZrC in B_h WC	2.4378E + 5	−6.4196E-2	−3.4118E-6	8.0488E-3

phase separation that can occur in the B1 structure. This conclusion was also found in the experimental work of Markström and Frisk who observed miscibility gaps between 1600 ∼ 1800 K for the TiC-ZrC-WC and VC-ZrC-WC systems [21].

The second observed trend is that T_{eqv} is lowered by including primarily group IVB metals as opposed to the group VB carbides. This is a result of the fact that $\bar{L}^{\alpha 0}_{M_iC-WC}$ is lower (more negative) and the term ΔG^{β}_{MC} is larger for the group IVB carbides. As noted in the analytical model, these trends will generally result in a lower T_{eqv}, or increased solubility of WC.

To illustrate the contribution of the configurational entropy to the HECs, both with and without WC, the calculated T_{eqv} is plotted with respect to the number of component carbides (N) in Fig. 7. Fig. 7(a) shows the trend of T_{eqv} that generally does not decrease with increasing number of elements. This trend indicates the significance of the mixing enthalpy which can easily compensate for the added entropy of additional components, indicating that enthalpy is as important (if not more important than) as the entropy. The trend can be further understood by noting that as we add more elements, we are more likely to add elements that increase the mixing enthalpy, compensating for the entropy. This plot does, however, exclude those that have negative mixing enthalpies, since those T_{eqv} values are zero. When WC is included, we do see a decrease in T_{eqv} with increasing number of elements, but the dependence is very weak beyond ternary solutions again indicating that entropy does not play a dominate role. Furthermore, none of the WC solutions are stable below 1500 K, indicating that the mixing enthalpy prevents the formation of a single-phase solid solution at or near room temperatures and does not govern stability of these compounds at room temperature.

4. Summary and conclusion

In this work, we studied the thermodynamic stability of equiatomic mixed carbides, or HECs, consisting of the group IVB, VB carbides (B1 structure) and WC (B_h structure) via the CALPHAD approach. The relevant thermodynamic data at finite temperatures was obtained from DFT calculations and the Debye-Grüneisen model. Our results show that, in general, the group IVB and VB carbides prefer to mix with carbides that have similar lattice constants which is a result of the positive correlation between the regular solution RK coefficients and the magnitude of the lattice constant differences. Our computed results for T_{eqv} reveals a strong dependence on the mixing enthalpy; the effect is so strong that increasing the number of elements does not, on average, decrease T_{eqv}. The is because as more elements are added, you increase the number of elements where mixing is unfavorable, leading to the increased

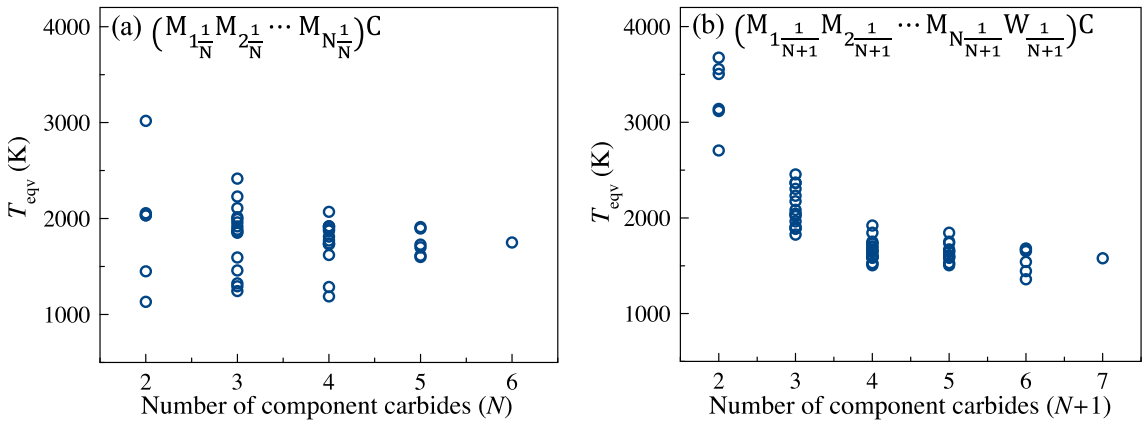

Fig. 7. The lower temperature limits T_{eqv} for the B1-structured single-phase equiatomic multicomponent carbides: (a) the mixed carbides not including WC, noted as $M_{1(1/N)}M_{2(1/N)}\cdots M_{N(1/N)}C$; (b) the mixed carbides including WC, noted as $M_{1[1/(N+1)]}M_{2[1/(N+1)]}\cdots M_{N[1/(N+1)]}W_{1/(N+1)}C$ where M_i represents the element in group IVB and VB.

temperature to form a single-phase solid solution that counteracts the increased entropy. Therefore, it would be inappropriate to call these materials 'high entropy carbides' as entropy does not stabilize these compounds. The stability is largely controlled by the mixing enthalpy.

Since WC prefers the B_h structure at low temperatures, the inclusion of WC generally increases the temperature to form an equiatomic solid solution. However, if WC is included in the solution, the minimum solution temperature (T_{eqv}) does show a moderate dependence on the number of elements for pseudo-ternary and lower component solutions. For more than three components, there is no apparent dependence on the number of components in the solution due to the variation in temperature caused by differences in the mixing enthalpy. Irrespective of the number of elements or the specific combinations chosen, the T_{eqv} values for solutions with WC do not drop below ~ 1500 K. Thus, it is not possible to thermodynamically stabilize WC in a so-called HEC at room temperature. This further suggests that these solutions, at least at low temperatures, do not have high entropy.

There are many experimentally synthesized HECs that are predicted in this work to be thermodynamically unstable. Therefore, our results may seem at odds with recently synthesized HECs that show that these elements are in a solid solution. However, our work does not suggest the systems are mechanically unstable and thus it is possible to trap elements into a thermodynamically metastable structure during synthesis. This is particularly important to realize because the decomposition of these materials, either through traditional nucleation and growth or spinodal decomposition, requires the diffusion of the metal atoms in the transition metal carbides. This could be particularly challenging because the metal atoms in transition metal carbides have very large activation energies, with values in the range of 5–7 eV as reported for TiC and ZrC [68,69]. Hence, at low temperatures, these metastable or unstable structures require metal atom diffusion to decompose and may be essentially kinetically 'locked-in'. Therefore, the processing of these materials, which facilitates the mixing, are likely important considerations in how well these materials can form solid solutions. For example, metastable solutions could be a result of the combination of mechanical mixing of small powders, high stresses during compaction, and surface thermodynamics, all of which could enhance mixing of the metal atom species prior to consolidation into a bulk phase. To sum up, our study here suggests that while mixing entropy is important in forming mixed transition metal carbides, it is not the main factor controlling their formation. Therefore, we doubt the term 'high entropy carbides' should be used to describe these materials and it is more appropriate to call them 'multiple principal component carbides' similar to multiple principal component alloys [70].

CRediT authorship contribution statement

Xiaochuan Tang: Conceptualization, Methodology, Software, Writing – original draft. **Gregory B. Thompson:** Conceptualization, Writing – review & editing. **Kaka Ma:** Conceptualization, Writing – review & editing. **Christopher R. Weinberger:** Conceptualization, Methodology, Data curation, Supervision, Project administration, Funding acquisition, Writing – review & editing.

Declaration of Competing Interest

The authors declare the following financial interests/personal relationships which may be considered as potential competing interests: Christopher R. Weinberger, Gregory B. Thompson reports financial support was provided by National Science Foundation.

Acknowledgement

This material is based upon work supported by the National Science Foundation under Grant No. NSF-DMR-2026760 and NSF-DMR-2026766. This work utilized the RMACC Summit supercomputer, which is supported by the National Science Foundation (awards ACI-1532235 and ACI-1532236), the University of Colorado Boulder and Colorado State University. The RMACC Summit supercomputer is a joint effort of the University of Colorado Boulder and Colorado State University.

Data Availability

All data underlying the results are available as listed in Appendix and *Supplemental Materials*, and no additional source data are required.

Appendix A. Supplementary data

Supplementary data to this article can be found online at https://doi.org/10.1016/j.commatsci.2022.111474.

References

[1] E. Wuchina, E. Opila, M. Opeka, B. Fahrenholtz, I. Talmy, UHTCs: Ultra-High Temperature Ceramic Materials for Extreme Environment Applications, Electrochem. Soc. Interface 16 (4) (2007) 30–36.
[2] R.A. Andrievskii, N.S. Strel'nikova, N.I. Poltoratskii, E.D. Kharkhardin, V. S. Smirnov, Melting point in systems ZrC-HfC, TaC-ZrC, TaC-HfC, Powder Metall. Met. Ceram. 6 (1) (1967) 65–67.
[3] C.R. Weinberger, G.B. Thompson, Review of phase stability in the group IVB and VB transition-metal carbides, J. Am. Ceram. Soc. 101 (10) (2018) 4401–4424.

[4] W.M. Mellor, K. Kaufmann, O.F. Dippo, S.D. Figueroa, G.D. Schrader, K.S. Vecchio, Development of ultrahigh-entropy ceramics with tailored oxidation behavior, J. Eur. Ceram. Soc. 41 (12) (2021) 5791–5800, https://doi.org/10.1016/j.jeurceramsoc.2021.05.010.

[5] D.G. Sangiovanni, F. Tasnádi, T. Harrington, M. Odén, K.S. Vecchio, I.A. Abrikosov, Temperature-dependent elastic properties of binary and multicomponent high-entropy refractory carbides, Mater. Des. 204 (2021) 109634, https://doi.org/10.1016/j.matdes.2021.109634.

[6] J. Pötschke, M. Dahal, M. Herrmann, A. Vornberger, B. Matthey, A. Michaelis, Preparation of high-entropy carbides by different sintering techniques, J. Mater. Sci. 56 (19) (Jul. 2021) 11237–11247, https://doi.org/10.1007/s10853-021-06004-y.

[7] R.-Z. Zhang, M.J. Reece, Review of high entropy ceramics: design, synthesis, structure and properties, J. Mater. Chem. A 7 (39) (2019) 22148–22162, https://doi.org/10.1039/C9TA05698J.

[8] E.P. George, D. Raabe, R.O. Ritchie, High-entropy alloys, Nat. Rev. Mater. 4 (8) (Aug. 2019) 515–534, https://doi.org/10.1038/s41578-019-0121-4.

[9] E.P. George, W.A. Curtin, C.C. Tasan, High entropy alloys: A focused review of mechanical properties and deformation mechanisms, Acta Mater. 188 (2020) 435–474.

[10] P.A. Korzhavyi, L.V. Pourovskii, H.W. Hugosson, A.V. Ruban, B. Johansson, Ab Initio Study of Phase Equilibria in TiCx, Phys. Rev. Lett. 88 (1) (Dec. 2001), 015505, https://doi.org/10.1103/PhysRevLett.88.015505.

[11] A. I. Gusev, A. A. Rempel, and A. J. Magerl, *Disorder and Order in Strongly Nonstoichiometric Compounds: Transition Metal Carbides, Nitrides and Oxides*. Berlin Heidelberg, Germany: Springer-Verlag Berlin Heidelberg, 2001. [Online]. Available: https://www.springer.com/gp/book/9783540418177.

[12] E. Castle, T. Csanádi, S. Grasso, J. Dusza, M. Reece, Processing and Properties of High-Entropy Ultra-High Temperature Carbides, Sci. Rep. 8 (1) (Jun. 2018) 8609, https://doi.org/10.1038/s41598-018-26827-1.

[13] J. Dusza, P. Švec, V. Girman, R. Sedlák, E.G. Castle, T. Csanádi, A. Kovalčíková, M. J. Reece, Microstructure of (Hf-Ta-Zr-Nb)C high-entropy carbide at micro and nano/atomic level, J. Eur. Ceram. Soc. 38 (12) (2018) 4303–4307, https://doi.org/10.1016/j.jeurceramsoc.2018.05.006.

[14] T. Csanádi, E. Castle, M.J. Reece, J. Dusza, Strength enhancement and slip behaviour of high-entropy carbide grains during micro-compression, Sci. Rep. 9 (1) (Jul. 2019) 10200, https://doi.org/10.1038/s41598-019-46614-w.

[15] X. Yang, Y. Zhang, Prediction of high-entropy stabilized solid-solution in multi-component alloys, Mater. Chem. Phys. 132 (2) (Feb. 2012) 233–238, https://doi.org/10.1016/j.matchemphys.2011.11.021.

[16] J. Zhou, J. Zhang, F. Zhang, B. Niu, L. Lei, W. Wang, High-entropy carbide: A novel class of multicomponent ceramics, Ceram. Int. 44 (17) (Dec. 2018) 22014–22018, https://doi.org/10.1016/j.ceramint.2018.08.100.

[17] T.J. Harrington, J. Gild, P. Sarker, C. Toher, C.M. Rost, O.F. Dippo, C. McElfresh, K. Kaufmann, E. Marin, L. Borowski, P.E. Hopkins, J. Luo, S. Curtarolo, D. W. Brenner, K.S. Vecchio, Phase stability and mechanical properties of novel high entropy transition metal carbides, Acta Mater. 166 (2019) 271–280, https://doi.org/10.1016/j.actamat.2018.12.054.

[18] A. Sedegov, S. Vorotilo, V. Tsybulin, K. Kuskov, D. Moscovskikh, Synthesis and study of high-entropy ceramics based on the carbides of refractory metals, IOP Conf. Ser. Mater. Sci. Eng. 558 (1) (2019) 012043.

[19] K. Wang, L. Chen, C. Xu, W. Zhang, Z. Liu, Y. Wang, J. Ouyang, X. Zhang, Y. Fu, Y. u. Zhou, Microstructure and mechanical properties of (TiZrNbTaMo)C high-entropy ceramic, J. Mater. Sci. Technol. 39 (2020) 99–105, https://doi.org/10.1016/j.jmst.2019.07.056.

[20] K. Frisk, Thermodynamic modelling of multicomponent cubic Nb, Ti and V carbides/carbonitrides, Calphad 32 (2) (2008) 326–337, https://doi.org/10.1016/j.calphad.2007.11.007.

[21] A. Markström, K. Frisk, Experimental and thermodynamic evaluation of the miscibility gaps in MC carbides for the C-Co–Ti–V–W–Zr system, Calphad 33 (3) (2009) 530–538, https://doi.org/10.1016/j.calphad.2009.03.002.

[22] B. Ye, T. Wen, M.C. Nguyen, L. Hao, C.-Z. Wang, Y. Chu, First-principles study, fabrication and characterization of (Zr0.25Nb0.25Ti0.25V0.25)C high-entropy ceramics, Acta Mater. 170 (May 2019) 15–23, https://doi.org/10.1016/j.actamat.2019.03.021.

[23] P. Sarker, T. Harrington, C. Toher, C. Oses, M. Samiee, J.-P. Maria, D.W. Brenner, K.S. Vecchio, S. Curtarolo, High-entropy high-hardness metal carbides discovered by entropy descriptors, Nat. Commun. 9 (1) (2018), https://doi.org/10.1038/s41467-018-07160-7.

[24] C. Servant, C.A. Danon, CALPHAD modelling of the unmixing of transition metal carbide phases, Calphad 28 (4) (2004) 337–353, https://doi.org/10.1016/j.calphad.2004.11.002.

[25] A. Markström, D. Andersson, K. Frisk, Combined ab-initio and experimental assessment of A1−xBxC mixed carbides, Calphad 32 (4) (Dec. 2008) 615–623, https://doi.org/10.1016/j.calphad.2008.07.014.

[26] V.I. Ivashchenko, P.E.A. Turchi, N.R. Medukh, V.I. Shevchenko, L. Gorb, J. Leszczynski, A first-principles study of the stability and mechanical properties of ternary transition metal carbide alloys, J. Appl. Phys. 125 (23) (2019) 235101, https://doi.org/10.1063/1.5096646.

[27] D. Sholl, J.A. Steckel, Density Functional Theory: A Practical Introduction. Hoboken, NJ, USA: Wiley, 2011. [Online]. Available: https://books.google.com/books?id=_f994dmAdv0C.

[28] V.N. Zharkov, V.A. Kalinin, Equations of State for Solids at High Pressures and Temperatures. Springer US, 1971. [Online]. Available: https://books.google.com/books?id=D6zvAAAAMAAJ.

[29] Y. Wang, R. Ahuja, B. Johansson, Mean-field potential approach to the quasiharmonic theory of solids, Int. J. Quantum Chem. 96 (5) (2004) 501–506, https://doi.org/10.1002/qua.10769.

[30] X.-G. Lu, M. Selleby, B. Sundman, Calculations of thermophysical properties of cubic carbides and nitrides using the Debye-Grüneisen model, Acta Mater. 55 (4) (2007) 1215–1226, https://doi.org/10.1016/j.actamat.2006.05.054.

[31] D. R. Gaskell, *Introduction to the Thermodynamics of Materials, Fifth Edition*. Taylor & Francis, 2003. [Online]. Available: https://books.google.com/books?id=YFgMRNjNtrgC.

[32] A. Cooper, *Mass Transport Phenomena in Ceramics*. Springer US, 2013. [Online]. Available: https://books.google.com/books?id=WYnAngEACAAJ.

[33] Y. A. Chang and W. A. Oates, *Materials Thermodynamics*. Wiley, 2010. [Online]. Available: https://books.google.com/books?id=lQr9pzZr7bgC.

[34] Z. K. Liu and Y. Wang, *Computational Thermodynamics of Materials*. Cambridge University Press, 2016. [Online]. Available: https://books.google.com/books?id=0J5ODAAAQBAJ.

[35] B. Alling, et al., Mixing and decomposition thermodynamics of c-Ti1-xAlxN from first-principles calculations, Phys. Rev. B 75 (4) (Jan. 2007), 045123, https://doi.org/10.1103/PhysRevB.75.045123.

[36] A.V. Ruban, S.I. Simak, S. Shallcross, H.L. Skriver, Local lattice relaxations in random metallic alloys: Effective tetrahedron model and supercell approach, Phys. Rev. B 67 (21) (Jun. 2003), 214302, https://doi.org/10.1103/PhysRevB.67.214302.

[37] P.E. Blöchl, Projector augmented-wave method, Phys. Rev. B 50 (24) (Dec. 1994) 17953–17979, https://doi.org/10.1103/PhysRevB.50.17953.

[38] G. Kresse, D. Joubert, From ultrasoft pseudopotentials to the projector augmented-wave method, Phys. Rev. B 59 (3) (Jan. 1999) 1758–1775, https://doi.org/10.1103/PhysRevB.59.1758.

[39] G. Kresse, J. Hafner, Ab initio molecular dynamics for liquid metals, Phys. Rev. B 47 (1) (Jan. 1993) 558–561, https://doi.org/10.1103/PhysRevB.47.558.

[40] G. Kresse, J. Furthmüller, Efficiency of ab-initio total energy calculations for metals and semiconductors using a plane-wave basis set, Comput. Mater. Sci. 6 (1) (1996) 15–50, https://doi.org/10.1016/0927-0256(96)00008-0.

[41] G. Kresse, J. Furthmüller, Efficient iterative schemes for ab initio total-energy calculations using a plane-wave basis set, Phys. Rev. B 54 (16) (Oct. 1996) 11169–11186, https://doi.org/10.1103/PhysRevB.54.11169.

[42] J.P. Perdew, K. Burke, M. Ernzerhof, Generalized Gradient Approximation Made Simple, Phys. Rev. Lett. 77 (18) (Oct. 1996) 3865–3868, https://doi.org/10.1103/PhysRevLett.77.3865.

[43] J.P. Perdew, J.A. Chevary, S.H. Vosko, K.A. Jackson, M.R. Pederson, D.J. Singh, C. Fiolhais, Atoms, molecules, solids, and surfaces: Applications of the generalized gradient approximation for exchange and correlation, Phys. Rev. B 46 (11) (1992) 6671–6687, https://doi.org/10.1103/PhysRevB.46.6671.

[44] A. van de Walle, M. Asta, G. Ceder, The Alloy Theoretic Automated Toolkit: A User Guide, Calphad 26 (4) (2002) 539–553, https://doi.org/10.1016/S0364-5916(02)80006-2.

[45] A. van de Walle, Multicomponent multisublattice alloys, nonconfigurational entropy and other additions to the Alloy Theoretic Automated Toolkit, Calphad 33 (2) (2009) 266–278, https://doi.org/10.1016/j.calphad.2008.12.005.

[46] J. C. Slater, *Introduction To Chemical Physics*. Read Books Limited, 2011. [Online]. Available: https://books.google.com/books?id=TDB8CgAAQBAJ.

[47] J.S. Dugdale, D.K.C. MacDonald, The Thermal Expansion of Solids, Phys. Rev. 89 (4) (Feb. 1953) 832–834, https://doi.org/10.1103/PhysRev.89.832.

[48] A.M. Krivtsov, V.A. Kuz'kin, Derivation of equations of state for ideal crystals of simple structure, Mech. Solids 46 (3) (2011) 387–399.

[49] D.H. Chung, W.R. Buessem, The Voigt-Reuss-Hill (VRH) Approximation and the Elastic Moduli of Polycrystalline ZnO, TiO\textsubscript2 (Rutile), and α-Al \textsubscript2O\textsubscript3, J. Appl. Phys. 39 (6) (1968) 2777–2782, https://doi.org/10.1063/1.1656672.

[50] Y. S. Touloukian, R. K. Kirby, E. R. Taylor, and T. Y. R. Lee, "Thermophysical properties of matter - the TPRC data series. Volume 13. Thermal expansion - nonmetallic solids. (Reannouncement). Data book," Jan. 1977, [Online]. Available: https://www.osti.gov/biblio/5438520.

[51] M. Chase, *NIST-JANAF Thermochemical Tables, 4th Edition*. American Institute of Physics, -1, 1998.

[52] W. Lengauer, S. Binder, K. Aigner, P. Ettmayer, A. Guillou, J. Debuigne, G. Groboth, Solid state properties of group IVb carbonitrides, J. Alloys Compd. 217 (1) (1995) 137–147, https://doi.org/10.1016/0925-8388(94)01315-9.

[53] K. Aigner, W. Lengauer, D. Rafaja, P. Ettmayer, Lattice parameters and thermal expansion of Ti(CxN1−x), Zr(CxN1−x), Hf(CxN1−x) and TiN1−x from 298 to 1473 K as investigated by high-temperature X-ray diffraction, J. Alloys Compd. 215 (1) (1994) 121–126, https://doi.org/10.1016/0925-8388(94)90828-1.

[54] E. K. Storms, *The Refractory Carbides [by] Edmund K. Storms*. Academic Press, 1967. [Online]. Available: https://books.google.com/books?id=fwyjtAEACAAJ.

[55] A.G. Turchanin, S.A. Babenko, B.V. Mitrofanov, N.V. Ivenko, Thermodynamic properties of hafnium oxycarbonitrides in the range of 298–1500 K, Zhurnal Fiz. Khimii 59 (7) (1985) 1847–1849.

[56] V.N. Lipatnikov, L.V. Zueva, A.I. Gusev, A. Kottar, Disorder-order phase transformations and electrical resistivity of nonstoichiometric titanium carbide, Phys. Solid State 40 (7) (Jul. 1998) 1211–1218, https://doi.org/10.1134/1.1130523.

[57] A.I. Gusev, A.A. Rempel, V.N. Lipatnikov, Heat capacity of niobium and tantalum carbides NbCy and TaCy in disordered and ordered states below 300 K, Phys. Status Solidi B 194 (2) (1996) 467–482.

[58] W. Huang, M. Selleby, Thermodynamic Assessment of the Nb–W–C System, Int. J. Mater. Res. 88 (1) (1997) 55–62, https://doi.org/10.3139/ijmr-1997-0010.

[59] R.H. Willens, E. Buehler, The superconductivity of the monocarbides of tungsten and molybdenum, Appl. Phys. Lett. 7 (1) (1965) 25–26, https://doi.org/10.1063/1.1754239.
[60] R.H. Willens, E. Buehler, B.T. Matthias, Superconductivity of the Transition-Metal Carbides, Phys. Rev. 159 (2) (Jul. 1967) 327–330, https://doi.org/10.1103/PhysRev.159.327.
[61] R.J.L. Andon, J.F. Martin, K.C. Mills, T.R. Jenkins, Heat capacity and entropy of tungsten carbide, J. Chem. Thermodyn. 7 (11) (1975) 1079–1084, https://doi.org/10.1016/0021-9614(75)90241-4.
[62] R. Otis, Z.-K. Liu, pycalphad: CALPHAD-based Computational Thermodynamics in Python, JORS 5 (1) (2017) 1, https://doi.org/10.5334/jors.140.
[63] H. Holleck, Ternary carbide systems of the refractory transition metals Pt 1, Metall 35 (10) (1981) 999–1004.
[64] S.V. Rempel, A.I. Gusev, Low-temperature decomposition and segregation on a surface in carbide-containing solid solutions of the zirconium–niobium–carbon system and in related ternary systems, Phys. Chem. Chem. Phys. 22 (26) (2020) 14918–14931, https://doi.org/10.1039/D0CP02074E.
[65] R. Kieffer, H. Nowotny, A. Neckel, P. Ettmayer, L. Usner, Zur Entmischung von kubischen Mehrstoffcarbiden, Monatshefte Für Chem. Chem. Mon. 99 (3) (May 1968) 1020–1027, https://doi.org/10.1007/BF00913751.
[66] H. Yu, M. Bahadori, G.B. Thompson, C.R. Weinberger, Understanding dislocation slip in stoichiometric rocksalt transition metal carbides and nitrides, J. Mater. Sci. 52 (11) (2017) 6235–6248.
[67] N. De Leon, X. Yu, H. Yu, C.R. Weinberger, G.B. Thompson, Bonding Effects on the Slip Differences in the B1 Monocarbides, Phys. Rev. Lett. 114 (16) (Apr. 2015), 165502, https://doi.org/10.1103/PhysRevLett.114.165502.
[68] S. Sarian, Diffusion of 44Ti in TiCx, J. Appl. Phys. 40 (9) (Aug. 1969) 3515–3520, https://doi.org/10.1063/1.1658229.
[69] R. Andrievskii, Y. Khromov, I. Alekseeva, Self-Diffusion of Carbon and Metal Atoms in Zirconium and Niobium Carbides, Fiz Met. Met. 32 (1971) Jan.
[70] O.N. Senkov, J.D. Miller, D.B. Miracle, C. Woodward, Accelerated exploration of multi-principal element alloys with solid solution phases, Nat. Commun. 6 (1) (Mar. 2015) 6529, https://doi.org/10.1038/ncomms7529.